D–A–CH – Mitteilungsblatt – Erdbebeningenieurwesen und Baudynamik

Eine gemeinsame Publikation von

D G E B
Deutsche Gesellschaft für Erdbebeningenieurwesen und Baudynamik
www.dgeb.eu

O G E
Österreichische Gesellschaft für Erdbebeningenieurwesen und Baudynamik
www.oge.or.at

S G E B
Schweizer Gesellschaft für Erdbebeningenieurwesen und Baudynamik
www.sgeb.ch

ISSN 1434–6591

Inhalt

Liebe Leserinnen,
liebe Leser,

durch die COVID-19 Pandemie, mussten die meisten der geplanten Aktivitäten, wie Fachtagungen und Kolloquien, weitestgehend in das 2021 verschoben werden. Diese Ausgabe gibt einen kurzen Bericht über die anstehenden Umplanungen und kommende Aktivitäten.

Das im Juli 2020 geplante D-A-CH-Doktorandenkolloquium in Kiel wird in den Juli 2021 verschoben. Als Vortragsgast konnte Emeritus Prof. Dimitri E. Beskos von der Universität Patras und derzeitiger Lehrstuhlleiter des Departments of Disaster Mitigation an der Tongji Universität, gewonnen werden. Er wird zum Thema „A performance-based hybrid force / displacement seismic design method for steel, reinforced concrete and composite frames“, referieren. Eine Einladung an die D-A-CH-Organisationen und -Forschungsinstitute wird Ende 2020 versendet. Eingeladen sind alle interessierten Doktoranden der Gebiete Baudynamik und Erdbebeningenieurwesen.

Im September 2021 wird die 17. D-A-CH-Tagung Erdbebeningenieurwesen und Baudynamik, die von der OGE, DGEB und SGEB organisiert wird, an der ETH Zürich stattfinden.

In dieser Ausgabe des D-A-CH-Mitteilungsblatts widmen sich wieder spezielle Arbeiten der Baudynamik und des Erdbebeningenieurwesens unterschiedlichen Fachthemen. Eine Publikation beschäftigt sich mit der Analyse des dynamischen Boden-Bauwerk-Interaktionsverhaltens von Integralbrücken. Es wird eine Methodik zur Einbettung von Bodenstrukturen in kommerzielle FEM-Programme, wie ABAQUS, durch die Bildung eines Makro-Finiten-Elements vorgestellt. Die Bodenstruktur wurde dabei durch Randelemente abgebildet. Anhand von unterschiedlichen Interaktionssimulationen wird der wesentliche Einfluss des Untergrundes auf das Eigenschwingverhalten der Brücke dargestellt. Ein weiterer Beitrag analysiert Verbund-Scherwände für Hochhäuser. Dazu werden neue Stahl-Beton-Verbundwände mit einem eingebetteten Stahlrahmen untersucht, um sowohl die Biegefestigkeit der Wand als auch die Scherfestigkeit der Stahlstreben zu verbessern. Anhand einer Vielzahl von Fallsimulationen wird die Wirkungsweise demonstriert.

Wenn Sie zur Diskussion der Fachaufsätze in dieser oder früheren Ausgaben beitragen möchten, so sind Sie herzlich dazu eingeladen. Ebenso sind Sie herzlich eingeladen, mit einem eigenen Aufsatz aus dem Gebiet des Erdbebeningenieurwesens und der Baudynamik den Fokus auf eine spezielle Thematik zu lenken. Bitte wenden Sie sich hierzu direkt an die Herausgeber. Entsprechende Informationen über die drei Gesellschaften und deren Kontaktdaten finden Sie auf den Internetseiten:

www.dgeb.org
www.oge.or.at
www.sgeb.ch

Eine anregende Lektüre wünschen Ihnen

Frank Wuttke,
Günther Achs und
Pia Hannewald.

Frank Wuttke
(Vorsitzender DGEB)

Günther Achs
(Generalsekretär OGE)

Pia Hannewald
(Präsidentin SGEB)

A numerical study on the influences of underlying soil and backfill characteristics on the dynamic behaviour of typical integral bridges

H. D. B. Aji, M. B. Basnet, F. Wuttke

ABSTRACT The identification of the dynamic behaviour of a structure is one of the crucial steps in the design of the dynamic resistance of the structure. The dynamic behaviour is represented by the natural frequencies and damping which are subsequently used along with the considered dynamic actions in the design process. In regard of integral bridge concept, one of the consequences of the omission of joints and bearings is the substantial soil-structure interaction which in turn increases the sensitivity of the dynamic behaviour of the bridges to the surrounding soil characteristic. In this article, we extended our hybrid BEM-FEM steady-state dynamic numerical tool to the 3D regime, developed by utilizing an in-house BEM and the commercial FEM software ABAQUS and use it to analyse the dynamic interaction between the bridge and the underlying soil as well as the backfill. The numerical results from four typical integral bridges show that underlying soil characteristic has great effect on the resonant frequencies and the damping. The backfill material properties tend to have less significant role due to the abutment wingwalls dominating the force transfer between the soil and the superstructure. The results also show that the degree of influence of the soil-structure interaction on the coupled system is affected by the type of load pattern in addition to the flexural stiffness of the superstructure.

1 Introduction

1.1 General notes on manuscript creation

Integral bridge concept was developed to overcome the maintenance as well as performance problems that were caused by the degradation or failure of movable joints and/or bearings. Despite its role in eliminating or reducing the stresses due to lateral movement and forces, joints and bearing are commonly not durable, less redundant, expensive to maintain and its non-performance can lead to collateral damages [19], [22]. The integral concept is realized by building monolithically the superstructure with its supporting substructure, that means abutments or piers, thus, eliminating the need for joints or bearings. Although studies showed that the application of integral bridge concept can have advantages such as economically better in the initial and long-term phases, better performance during earthquake, simpler construction and better vehicular experience [2], [3], [10], [17], its behaviour is not fully understood and agreed by members of scientific community, engineers as well as regulators.

One of the distinct points of the behaviour of integral bridges is the strong soil-structure interaction which occur due to the continuity of the bridge structural members and its contact to the adjacent backfill and underlying soil, especially in the case of short span or high stiffness superstructure. From the standpoint of dynamic-resistant design, the integral bridge dynamic characteristic, quantified through the natural frequencies and damping ratio of the system, cannot be assessed in the same manner as non-integral ones.

Some of the studies regarding the influence of soil-structure interaction on the dynamic response of bridges were those in [23], [24], [25]. In [12] and [13], studies regarding the influence of abutments and soil nonlinearities can be found. An earlier study by [18], using 3D BEM in frequency domain, investigated the stiffness of vertical walls of abutment and wingwalls, in contact with embankment, without the contribution of the vertical resistance from the soil under the foundation of the abutment. A simplified method of the abutment stiffness is sometimes preferred to reduce computational burden such as in [16]. Results of numerical-analytical approach where the soil reactions are represented by combination of translational and rotational springs can be found in [20] while a 3D time history FEM of a semi-integral bridge can be found in [5]. The sensitivity of the bridge seismic response with respect to different bridge modelling approaches were studied by using FEM and nonlinear springs in [4]. Later, more complex model were compared to simpler ones in [9] where, besides nonlinear hysteretic springs, dashpots and soil column were used to model radiation damping and free-field motion of nearby soil, respectively. These studies showed that mode shapes, natural frequencies, ultimate base shear strength and peak displacement were altered by the models. A study by [15] which combines field measurement as well as FEM and FEM-BEM results on short-span railway integral bridge found that the effect of surrounding soil to the response depends on the ratio between the flexural stiffness of the bridge and the dynamic stiffness of the foundation-soil system and to the ratio between resonant frequeny of the soil layer and the fundamental frequency of the bridge. The study also showed the modelling limitation that is currently experienced by the existing available numerical procedure which may affect the accuracy of the computation.

In this study, a 3D hybrid BEM-FEM approach is taken to assess the influence of the underlying soil and backfill material properties to the dynamic behaviour of typical integral bridges, expressed by the resonance frequencies of the coupled system, and comparison to the results obtained via conventional method, where a combination of encastré grounding and frequency-independent springs is used, are presented. Four typical single-span integral abutment bridges are analysed in steady-state dynamic manner for this study. In addition, the effects of span length and

curved alignment are also explored. The current study is focused on the system identification of the bridge-soil system rather than the ultimate capacity and thus, material and geometric nonlinearities are not considered.

The bridge superstructure, abutments and the backfill behind the abutments are modelled by using FEM, which is chosen due to its modelling accessibility, extensive element library as well as its efficiency to model complex structural system in finite domain. The underlying soil, on the other hand, is computed using BEM which can account for dynamic problem of unbounded domain and satisfy Sommerfeld's radiation condition in the far-field. The FEM tool used for this study is ABAQUS, which is also used as meshing tool for both subdomains, while the numerical BEM codes is an in-house code written in Matlab. The hybrid method used here is based on the FEM-hosted substructure approach in which the BEM equation is converted into FEM-compatible equation and attached to FEM model as a substructure element.

This article is organized as follows: a brief description of the formulation of BEM and FEM as well as the coupling procedure is given in section 2 followed by a validation of a numerical benchmark problem to an existing solution in section 3. In section 4, a detailed description of the typical integral bridges & the parameters considered in this study are given. The assessment results and discussions are given in section 5 followed by the conclusions in section 6.

2 Problem description

Let us consider a coupled system in **Figure 1**. An elastic isotropic semi-infinite geological region is denoted as Ω_{BEM} with boundary of $\Gamma_{BEM} = \Gamma_f = \Gamma_i$ and material properties of $C_{1(BEM)}$ & $C_{2(BEM)}$, which are the longitudinal and shear wave velocities. The boundary Γ_f is the free-surface of Ω_{BEM} whilst the Γ_i is the contact interface between Ω_{BEM} and Ω_{FEM}. The Ω_{FEM} is the finite continuum with surface Γ_{FEM} and material properties $C_{1(FEM)}$ & $C_{2(FEM)}$. Thus, Ω_{BEM} represents the surrounding media up to the far-field region while Ω_{FEM} represents the structure and can include near-field object such as, in this case study, soil back filling.

2.1 Hybrid BEM-FEM formulation of the boundary value problem

In this section, only a brief description of the formulations is given since classical formulations of both BEM and FEM are used through the steady-state dynamic coupling. For the semi-infinite domain Ω_{BEM}, bounded by the traction-free surface Γ_f and the interface Γ_i, the formulation of the boundary value problem given a circular frequency ω can be represented by the following integral equation, as given in [7]:

$$c_{lk}u_k^{\Omega_{BEM}}(x,\omega) = \int_{\Gamma_{BEM}} U_{lk}^{*\Omega_{BEM}}(x,\xi,\omega)t_k^{\Omega_{BEM}}(\xi,\omega)d\Gamma - \int_{\Gamma_{BEM}} T_{lk}^{*\Omega_{BEM}}(x,\xi,\omega)u_k^{\Omega_{BEM}}(\xi,\omega)d\Gamma , \quad (1)$$

where the 3D elastodynamic fundamental solution for displacement is

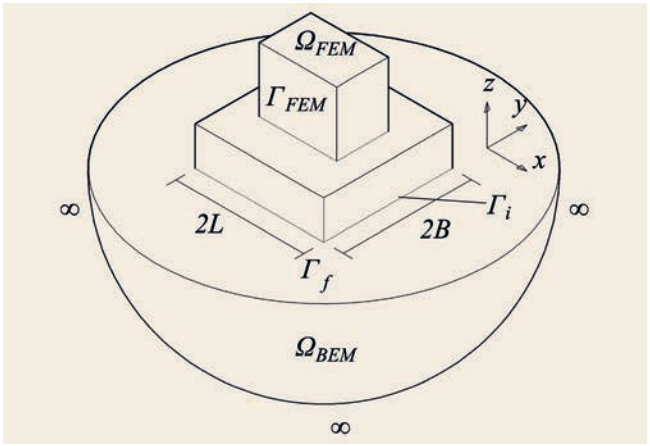

Fig. 1. Problem illustration of the 3D hybrid BEM-FEM model
Source: H. D. B. Aji, M. B. Basnet, F. Wuttke

$$U_{lk}^{*\Omega_{BEM}}(x,\xi,\omega) = \frac{1}{\alpha\pi\rho C_{2(BEM)}^2}\left[\Psi\delta_{lk} - \chi r_{,l}r_{,k}\right];$$

and its counterpart for traction is

$$T_{lk}^{*\Omega_{BEM}}(x,\xi,\omega) = \frac{1}{\alpha\pi}\left[\left(\frac{d\psi}{dr} - \frac{1}{r}\chi\right)\left(\delta_{lk}\frac{\partial r}{\partial n} + r_{,k}n_l\right) - \frac{2}{r}\chi\left(n_k r_l - 2r_{,l}r_{,k}\frac{\partial r}{\partial n}\right) - \frac{2dx}{dr}r_{,l}r_{,k}\frac{\partial r}{\partial n} + \left(\frac{C_{2(BEM)}^2}{C_{1(BEM)}^2} - 2\right)\left(\frac{d\psi}{dr} - \frac{dx}{dr} - \frac{\alpha}{2r}\chi\right)r_{,l}n_k\right].$$

Here, c_{lk} is a constant, which depends upon the geometry of the collocation point located at coordinate x. Various methods can be used to compute the value of this constant matrix, for example by the rigid body motion principle or by solving the traction fundamental solution over augmented spherical boundary covering the calculated point [7]. In this study, the latter analytical approach is derived and implemented for smooth and non-smooth points in 3D space. The notations t and u are the traction and displacement field of the boundary node. The boundary conditions on the traction-free surface is denoted as $t_f^{\Omega_{BEM}} = 0$.

After applying the discretization and collocation procedure, equation (1) is written as

$$\mathbf{H}^{\Omega_{BEM}}\mathbf{u}^{\Omega_{BEM}} = \mathbf{G}^{\Omega_{BEM}}\mathbf{t}^{\Omega_{BEM}}, \quad (2)$$

where $\mathbf{H}^{\Omega_{BEM}}$ and $\mathbf{G}^{\Omega_{BEM}}$ are the influence matrices; and $\mathbf{t}^{\Omega_{BEM}}$ and $\mathbf{u}^{\Omega_{BEM}}$ are the vectors of nodal displacement and traction, respectively. Equation (3) can be decoupled based on the nodes along the free-surface Γ_f and nodes along the subdomain interface Γ_i. It is subsequently solved into equation relating the nodal traction and displacement of the nodes along the interface following the procedure described in [21]. The equation now reads

$$\mathbf{t}_i^{\Omega_{BEM}} = \mathbf{B}\mathbf{u}_i^{\Omega_{BEM}}, \quad (3)$$

where $\mathbf{t}_i^{\Omega_{BEM}}$ and $\mathbf{u}_i^{\Omega_{BEM}}$ are the vectors of nodal traction and displacement of nodes along the interface, respectively; and $\mathbf{B}$ is described as follows:

$$\mathbf{B} = \left[\mathbf{G}_{ii}^{\Omega_{BEM}} - \mathbf{H}_{if}^{\Omega_{BEM}}\mathbf{A}_\mathbf{t}\right]^{-1}\left(\mathbf{H}_{ii}^{\Omega_{BEM}} - \mathbf{H}_{if}^{\Omega_{BEM}}\mathbf{A}_\mathbf{u}\right); \quad (4)$$

$$\mathbf{A}_\mathbf{t} = \left[\mathbf{H}_{ff}^{\Omega_{BEM}}\right]^{-1}\mathbf{G}_{fi}^{\Omega_{BEM}}; \quad \mathbf{A}_\mathbf{u} = \left[\mathbf{H}_{ff}^{\Omega_{BEM}}\right]^{-1}\mathbf{H}_{fi}^{\Omega_{BEM}}. \quad (5)$$

The $\mathbf{H}$ and $\mathbf{G}$ matrices in equations (3) and (4)] above are the decoupled products of equation (2) and the notation „*i*" refers to the nodes along the interface whilst notation „*f*" refers to

the free-surface. Equation (3) can be further made into FEM-compatible form by applying the transformation matrix $\mathbf{M}^*$, which maps nodal traction into nodal force, in the following manner:

$$\tilde{\mathbf{f}}_i^{\Omega_{BEM}} = \left[\mathbf{M}^*\right]\mathbf{B}\mathbf{u}_i^{\Omega_{BEM}} = \mathbf{K}^{\Omega_{BEM}}\mathbf{u}_i^{\Omega_{BEM}}, \quad (6)$$

where $\mathbf{K}^{\Omega_{BEM}}$ is the complex-valued stiffness matrix of the BEM subdomain.

For the finite domain Ω_{FEM}, the equation of motion for the steady-state problem for a circular frequency ω reads

$$\left[-\omega^2\mathbf{M}^{\Omega_{FEM}} + i\omega\mathbf{C}^{\Omega_{FEM}} + \left(\mathbf{K}^{\Omega_{FEM}} + i\mathbf{K}_s^{\Omega_{FEM}}\right)\right]\mathbf{u}^{\Omega_{FEM}} = \tilde{\mathbf{f}}^{\Omega_{FEM}}, \quad (7)$$

where $i = \sqrt{-1}$; $\mathbf{M}^{\Omega_{FEM}}$, $\mathbf{C}^{\Omega_{FEM}}$, $\mathbf{C}^{\Omega_{FEM}}$ and $\mathbf{K}^{\Omega_{FEM}}$ are the mass, damping and stiffness matrices, respectively; $\mathbf{K}_s^{\Omega_{FEM}}$ is the structural damping matrix; and $\tilde{\mathbf{f}}^{\Omega_{FEM}}$ is the nodal force vector. The compatibility between Ω_{BEM} and Ω_{FEM} at interface Γ_i is enforced through the conditions of traction $t_i^{\Omega_{BEM}} = -t_i^{\Omega_{FEM}}$ and displacement $u_i^{\Omega_{BEM}} = u_i^{\Omega_{FEM}}$.

To proceed with the coupling, equation (6) can be merged into equation (7) by superposition of the component of matrix into stiffness matrix $\mathbf{K}^{\Omega_{BEM}}$ assembly of Ω^{FEM} at the common nodes along the interface. The coupled equation reads

$$\left[-\omega^2\mathbf{M}^{\Omega_{FEM}} + i\omega\mathbf{C}^{\Omega_{FEM}} + (\mathbf{K} + i\mathbf{K}_s)\right]\mathbf{u}^{\Omega_{FEM}} = \tilde{\mathbf{f}}^{\Omega_{FEM}}, \quad (8)$$

where

$$\mathbf{K} = \mathbf{K}^{\Omega_{FEM}} + \mathbf{K}_{Re}^{\Omega_{BEM}}; \quad (9)$$

$$\mathbf{K}_s = \mathbf{K}_s^{\Omega_{FEM}} + \mathbf{K}_{Im}^{\Omega_{BEM}}. \quad (10)$$

The matrices $\mathbf{K}_{Re}^{\Omega_{BEM}}$ and $\mathbf{K}_{Im}^{\Omega_{BEM}}$ are simply the real and imaginary part of $\mathbf{K}^{\Omega_{BEM}}$, respectively.

2.2 Implementation of BEM as substructure element in ABAQUS

The coupling procedure follows the method for 2-dimensional case in [6]. The modelling starts with the use of ABAQUS pre-processing tool to model the geometry and to mesh the whole domain including BEM subdomain for which 4- or 8-nodes element are generated using shell element definition. These element nodal configurations are subsequently used as BEM elements in the in-house MATLAB code where computation, condensation and transformation of the BEM matrices are performed. The results are equivalent force and stiffness matrices. The stiffness matrices are then generated as substructure element using ABAQUS substructure generation procedure [1]. The resulted substructure element is later combined into the FEM model and the global equation is solved using the ABAQUS steady-state dynamics solver. The combined stiffness and structural damping matrices are thus unsymmetric and unbanded. No symmetrisation procedure is used since it may reduce the result quality.

3 Validation

To validate the numerical procedure, comparison of the hybrid computation results to the existing analytical solution for the case of the dynamic response of rigid massless foundation on homogeneous elastic isotropic half-space to time-harmonic excitation is performed. Consider the geometry as presented in Figure 1 in which Ω_{FEM} is a rectangular rigid massless foundation with dimension of $2B$ & $2L$ resting on an elastic isotropic half-space Ω_{BEM}. Time-harmonic unit vertical force, horizontal force and rotational moment about y-axis, denoted as H, V, M_y and are applied to the center of the foundation. The dynamic steady-state impedance for external force at direction „l“ and response at direction „k“, S_{lk}, can be obtained by inversion of the displacement responses written as

$$\begin{bmatrix} S_{xx} & S_{xz} & S_{xr_y} \\ S_{zx} & S_{zz} & S_{zr_y} \\ S_{r_yx} & S_{r_yz} & S_{r_y} \end{bmatrix} = \begin{bmatrix} H & 0 & 0 \\ 0 & V & 0 \\ 0 & 0 & M_y \end{bmatrix} \begin{bmatrix} u_{xx} & u_{zx} & u_{r_yx} \\ u_{xz} & u_{zz} & u_{r_yz} \\ u_{xr_y} & u_{zr_y} & u_{r_y} \end{bmatrix}^{-1}, \quad (11)$$

where S_{lk} is complex valued, that means $S_{lk} = K_{lk} + i\omega L_{lk}$, and it can be decoupled into the dynamic stiffness, K_{lk}, and the radiation damping, L_{lk}. For this validation, the solutions published [11] are used as benchmarks and for the sake of comparison, K_{lk} & L_{lk} values are subsequently normalized by the static stiffness and damping constants in [11], respectively. The results are the frequency-dependent factors, k_{lk} and l_{lk} which are directly comparable to charts published in [11].

The impedance results of 3D hybrid BEM-FEM for vertical, horizontal and rotational cases are presented together with the mentioned charts in **Figure 2** and they are in general in a good agreement. The discrepancies found in the result may be attributed to the different interface definition in which the referenced study used the „relaxed boundary“ while the current study uses the rough interface. The low graphical quality of the classic paper in our possession might partially contribute to them, as well.

4 Simulation and Parametric Analysis

To evaluate the influence of span as well as curved alignment, four typical integral bridges are modelled. These are typical overhead crossing, single span concrete integral bridges with monolithic superstructure-abutment joints resting on a half-space shown in **Figure 3**. The spans are chosen as 35 m & 45 m which are then cross-combined with alignment sets of straight and curved, radius of 400 m (**Table 1**). Other geometrical dimensions are kept constant: the width of the bridge is 12 m; the abutment height and thickness are 7.6 m and 0.5 m, respectively, with wingwalls extending to 1 : 1 slope; the superstructure consists of a 30 cm thick deck and five T-girders distanced at 2.5 m with 1.6 m height and 1.0 m high diaphragm.

Two numerical approaches are utilized to illustrate the effect of modelling on the dynamic identification: (1) a hybrid BEM-FEM approach and (2) a conventional approach where encastré groundings (fixed restrains) are applied along the bottom centreline of the abutment (perpendicular to the traffic direction) and frequency-independent springs are applied to the walls of the abutment and wingwalls to represent the passive soil resistance, see Figure 3(b). In the hybrid numerical approach, the backfills are modelled as continuum and included in the FEM subdomain whilst it is left out of numerical model in the conventional one. In both approaches, the deck-diaphragm-girder system of the superstructure is meshed using integrated beam and shell elements whereas the abutments and the wingwalls are discretized using continuum elements. The BEM substructure, as a result of the far-field computation, is directly attached to the continuous sur-

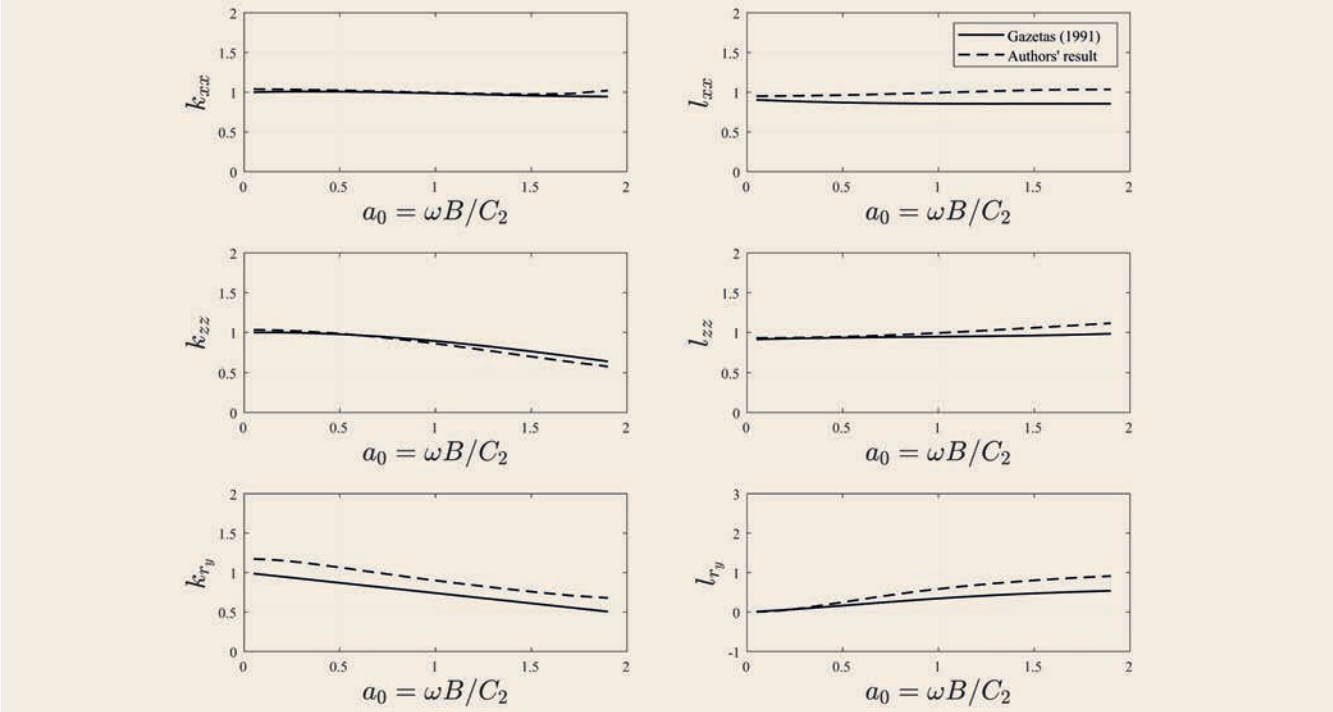

Fig. 2. Comparison of frequency-dependent factors for impedance functions of rectangular rigid massless foundation obtained by hybrid BEM-FEM with charts in [11] *Source: H. D. B. Aji, M. B. Basnet, F. Wuttke; [11]*

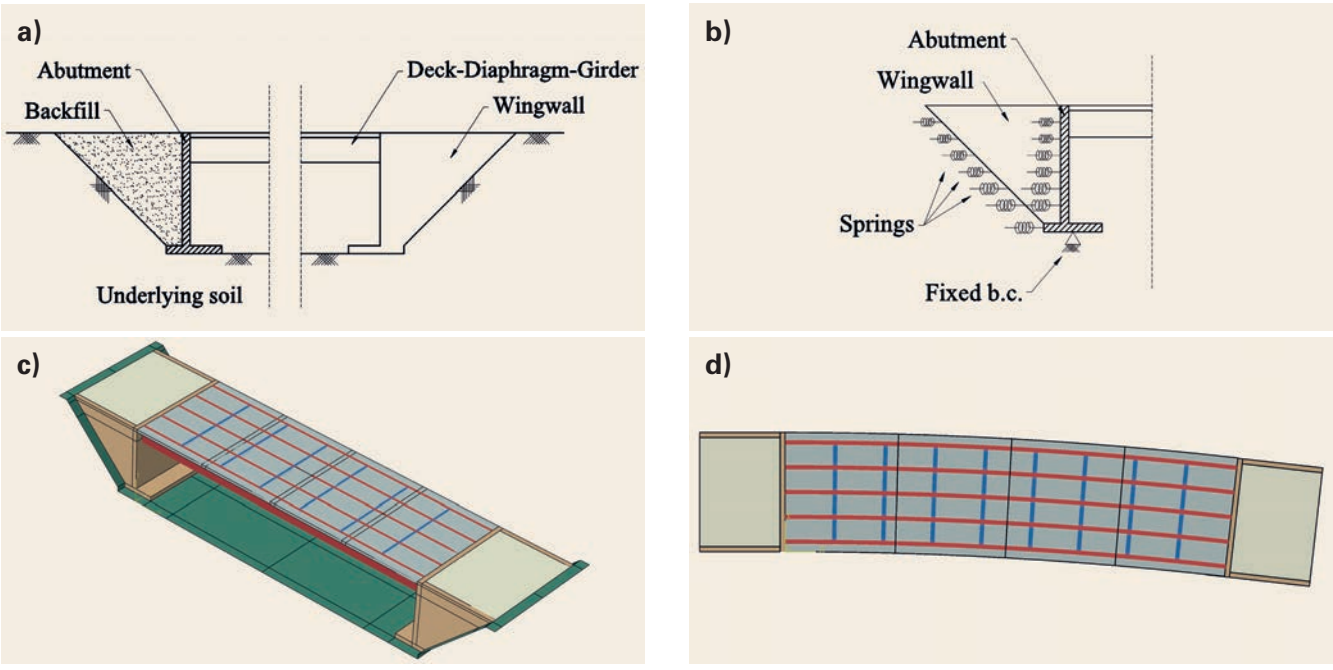

Fig. 3. Illustrations and views of the integral bridge model: (a) illustrative cross section of the hybrid approach, (b) illustrative cross section of the conventional approach, (c) isometric view of bridge model 1, and (d) top view of bridge model 4 *Source: H. D. B. Aji, M. B. Basnet, F. Wuttke*

face formed behind the wingwalls and backfills and under the spread footing. In Figure 3(c), the BEM subdomain prior to condensation is the green coloured surface.

The concrete properties of the bridge are as follows: Young's modulus of 300 GPa, Poisson's ratio of 0.2, and density of 2 400 kg/m^3. The underlying soil and backfill materials considered for the parametric analysis are laid out in **Table 2**. Poisson's ratio of 1/3 is assigned for all soil materials. The interface between the structure and backfill is of frictional type with friction angle 20°. The interface between the FEM and BEM subdomains is of tied constraint. For the study of the influence of the underlying soil, the no. 2 properties of Table 2 are assigned to the backfill whilst the properties of the underlying soil are varied. For the study of the influence of the backfill, the no. 2 properties are assigned to the underlying soil and the properties of the backfill are varied.

Table 1. Bridge models

No.	Span length (m)	radius of curvature (m)
1	35	∞
2	35	400
3	45	∞
4	45	400

Table 2. Material properties of the soil considered in the simulation

No.	C_2 (m/s)	ρ (kg/m³)	μ (MPa)
1	100	1 650	16.50
2	250	1 800	112.50
3	375	1 840	258.75
4	500	1 890	472.50

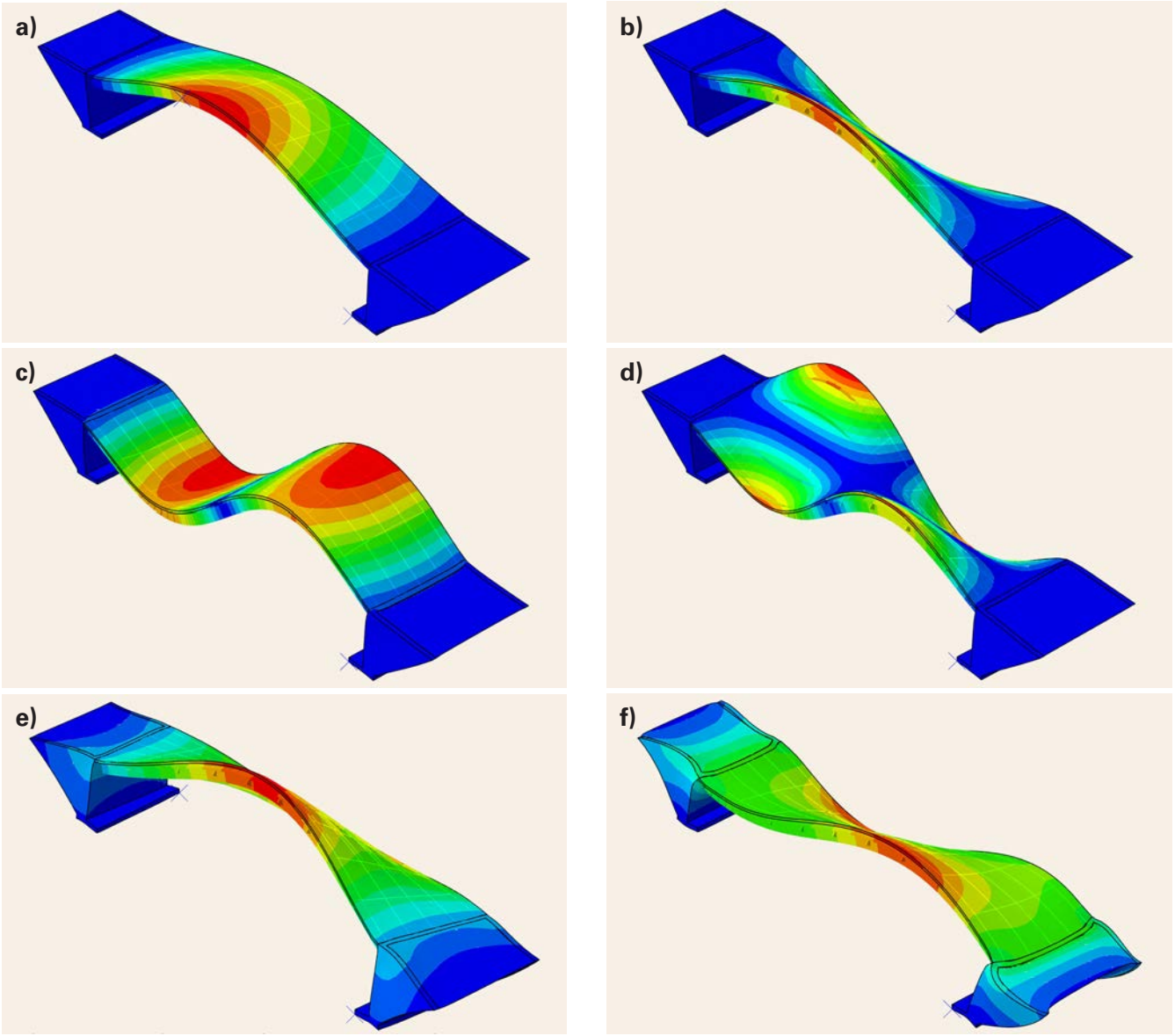

Fig. 4. Six mode shapes of the integral bridge considered in this study (bridge model 4): (a) mode 1, (b) mode 2, (c) mode 3, (d) mode 4, (e) mode 5, and (f) mode 6 *Source: H. D. B. Aji, M. B. Basnet, F. Wuttke*

In the conventional model, the spring values are computed following the lateral passive earth pressure according to Eurocode 7 using the following assumptions: (1) the density of the soil is 18 kN/m³; (2) the mode of wall movement is rotational one (i. e. type a of Table C.2 in [8]); (3) the calculation is based on the 1.1 % wall rotation to generate half mobilised passive resistance ($0.5\,\sigma_p$) of dense soil (Table C.2 of [8]); (4) the passive earth pressure coefficient is calculated based on Figure C.2.1 of [8]) with soil internal friction angle taken as 30° and the soil-wall friction angle taken as 20°.

For the conventional approach, the system identification is performed using eigenfrequency extraction whilst in the hybrid simulations, the resonant frequencies of the coupled system are generated by applying one- or multi-directional distributed load located at the deck. Six mode shapes that are considered in this study are shown in **Figure 4** for bridge model 4. For example,

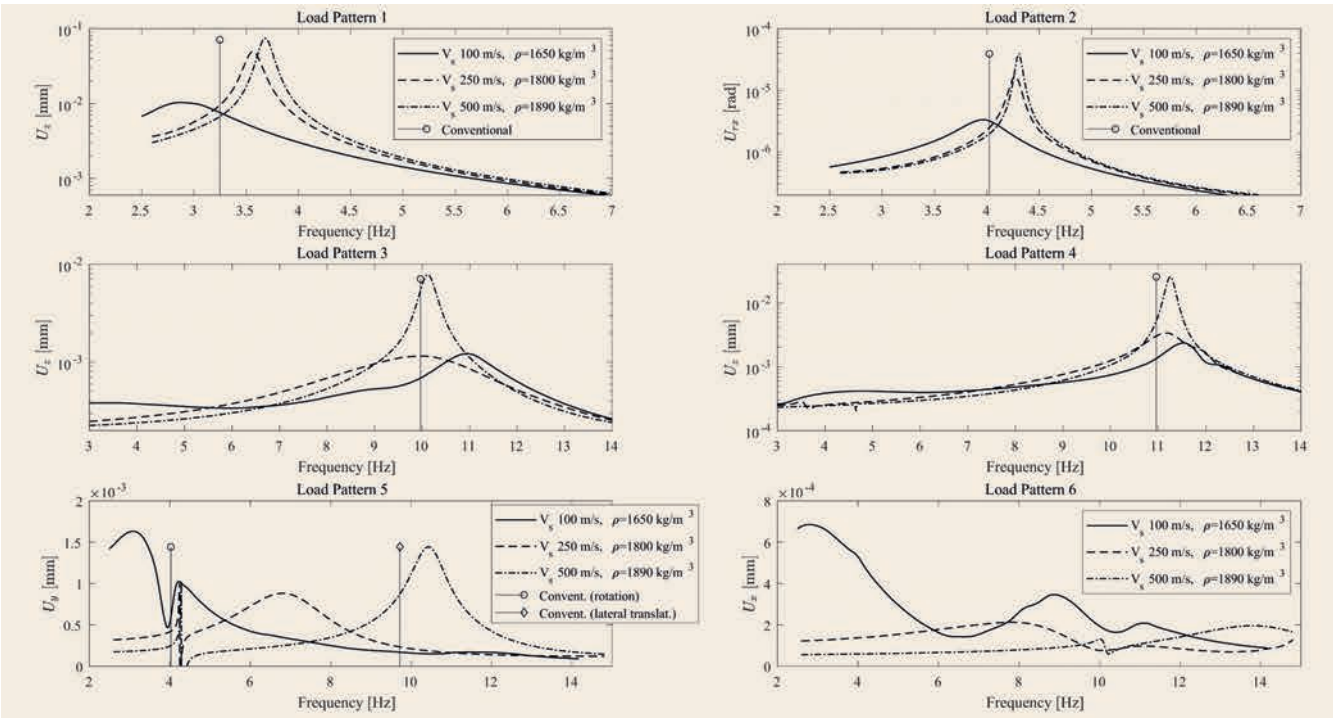

Fig. 5. Comparison of displacement response magnitude for six load patterns of bridge model 1 (L = 35 m, straight) with different underlying soil properties
Source: H. D. B. Aji, M. B. Basnet, F. Wuttke

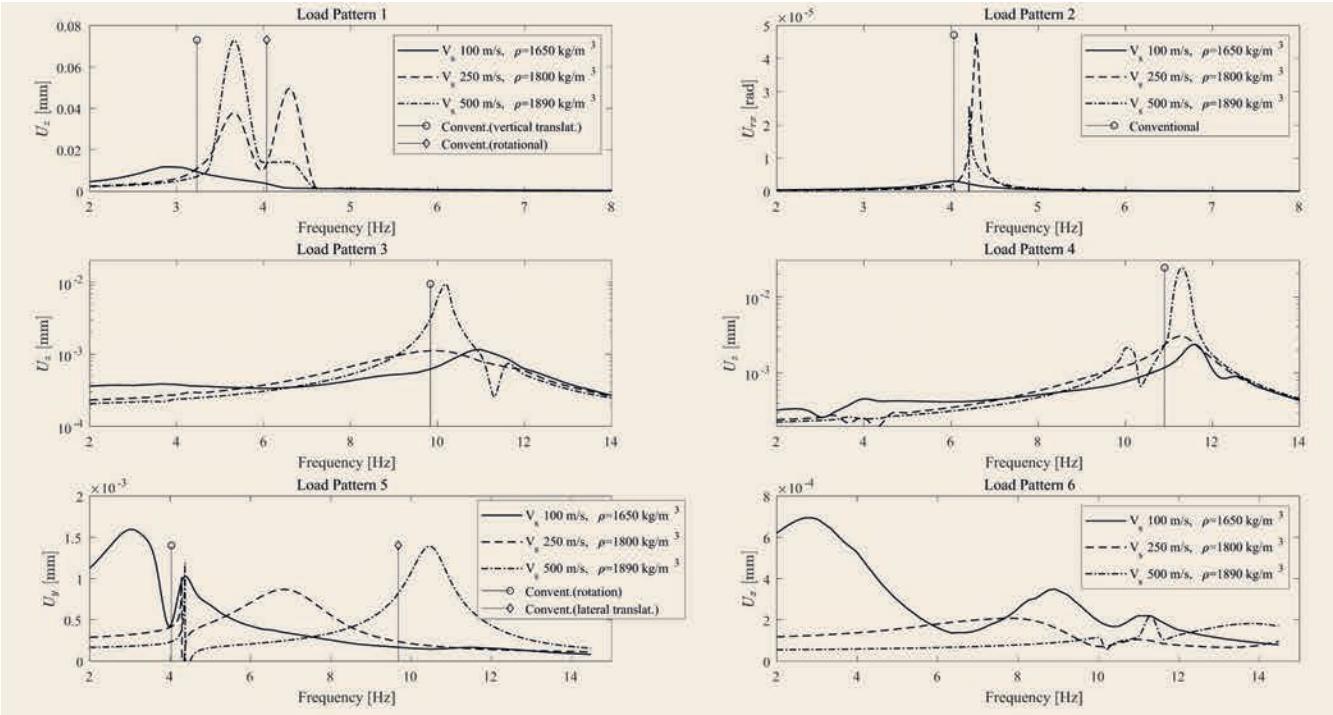

Fig. 6. Comparison of displacement response magnitude for six load patterns of bridge model 2 (L= 35 m, curved R = 400 m) with different underlying soil properties *Source: H. D. B. Aji, M. B. Basnet, F. Wuttke*

mode shape 1 is generated by uniform vertical distributed load while mode shape 2 is generated by coupled left-right vertical distributed load. The load patterns 5 and 6 are horizontal uniform distributed load in the transversal and longitudinal direction, respectively. The magnitude of the distributed load is 1 Pa. In each activated mode shape, the displacement is measured at the degree of freedom and the point at the deck which represents the maximum response consistently.

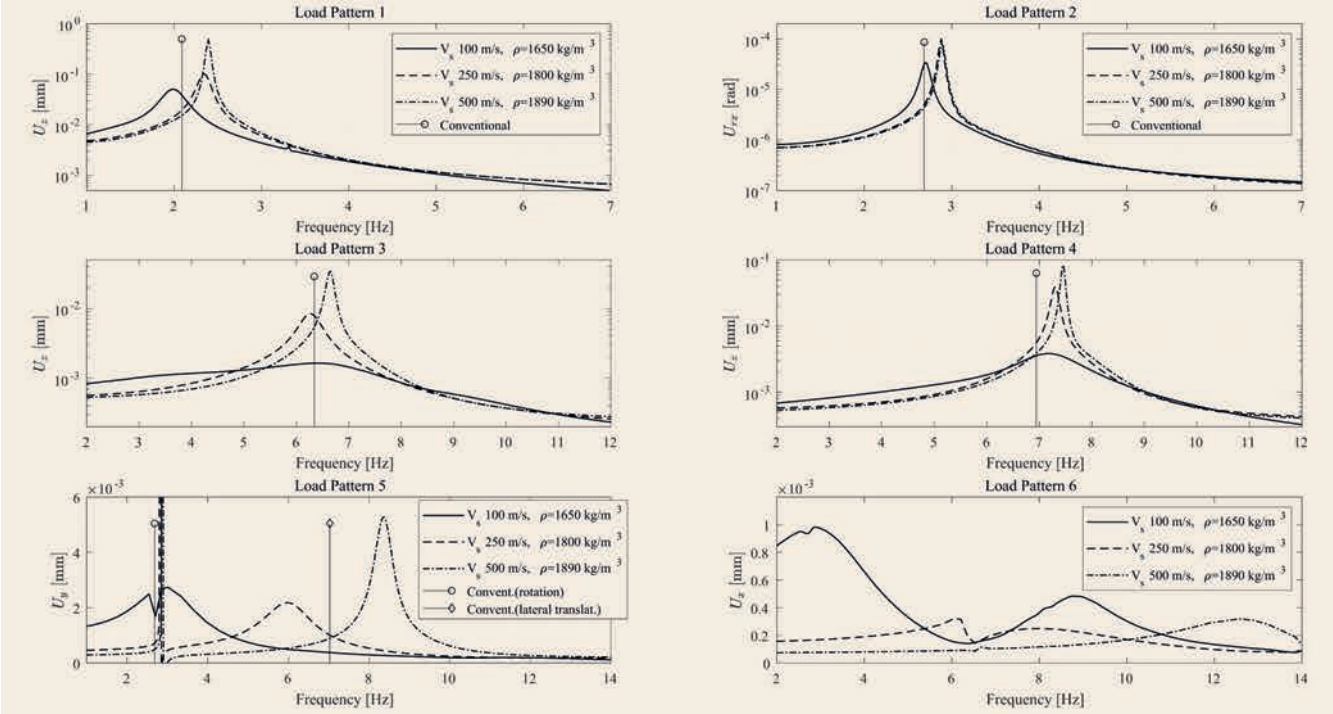

Fig. 7. Comparison of displacement response magnitude for six load patterns of bridge model 3 (L = 45 m, straight) with different underlying soil properties *Source: H. D. B. Aji, M. B. Basnet, F. Wuttke*

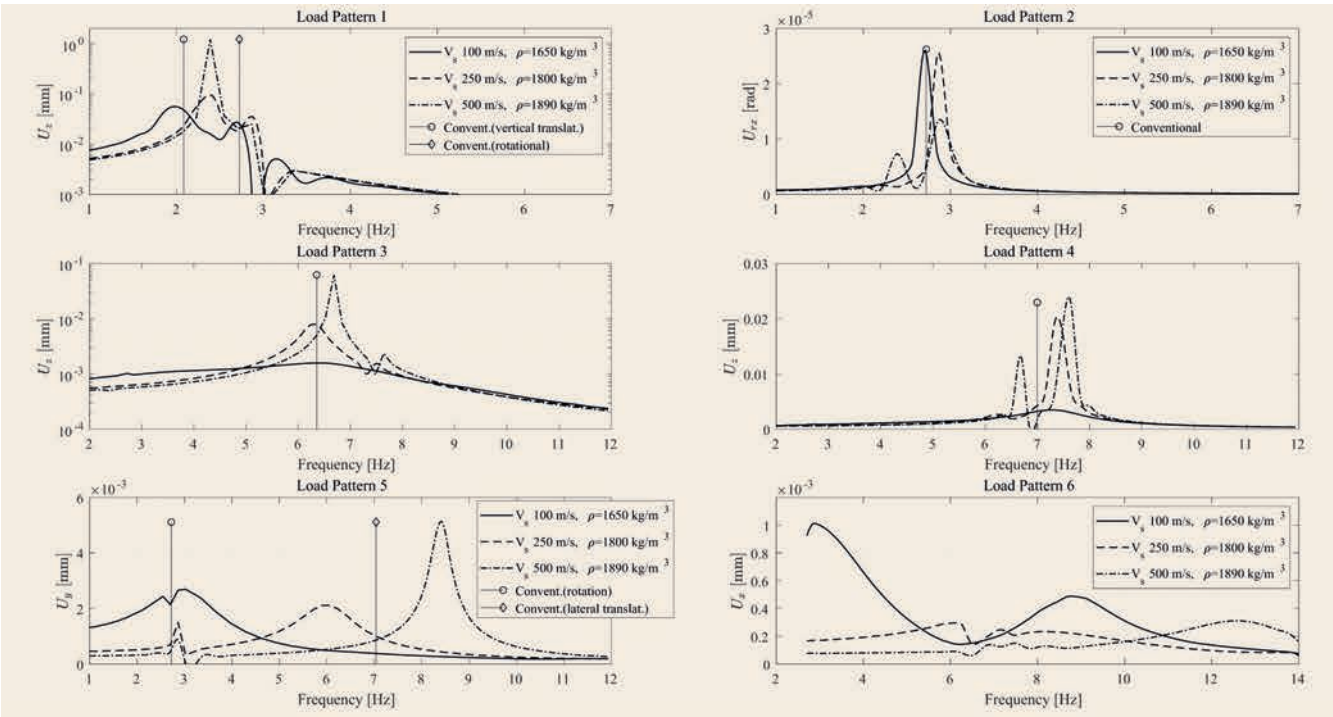

Fig. 8. Comparison of displacement response magnitude for six load patterns of bridge model 4 (L = 45 m, curved R = 400 m) with different underlying soil properties *Source: H. D. B. Aji, M. B. Basnet, F. Wuttke*

5 Results and discussion

The results for the simulations with varying underlying soil for each bridge model are presented in **Figure 5**, **Figure 6**, **Figure 7**, and **Figure 8** whilst the results for simulations with varying backfill are shown in **Figure 9**, **Figure 10**, **Figure 11**, and **Figure 12**. In these figures, the natural frequencies for corresponding mode shape obtained from conventional approach are presented as discrete plots and scaled for visibility. Load pattern 5 consistently generates two mode shapes: (1) rotational-dominant mode shape, found in the mode shape generated by load pattern 2 (Figure 4(b)), and (2) translational-dominant mode shape. No lon-

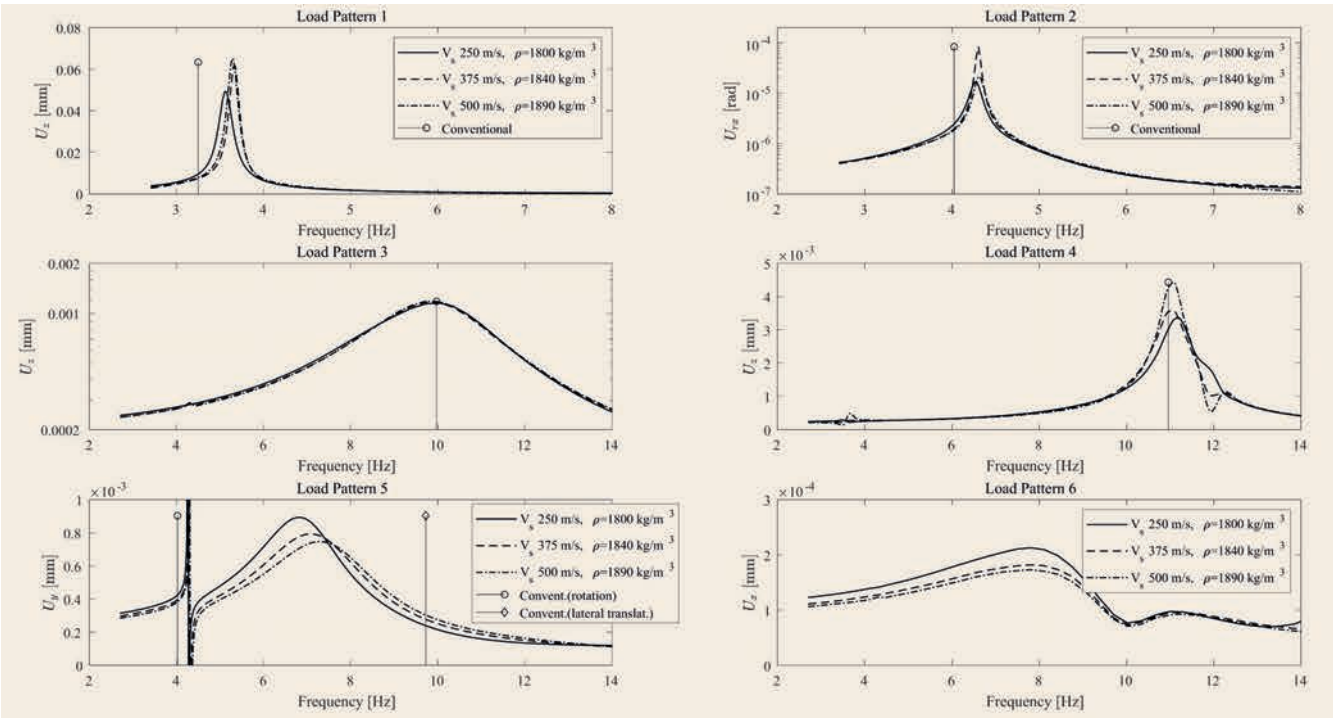

Fig. 9. Comparison of displacement response magnitude for six load patterns of bridge model 1 (L = 35 m, straight) with different backfill soil properties
Source: H. D. B. Aji, M. B. Basnet, F. Wuttke

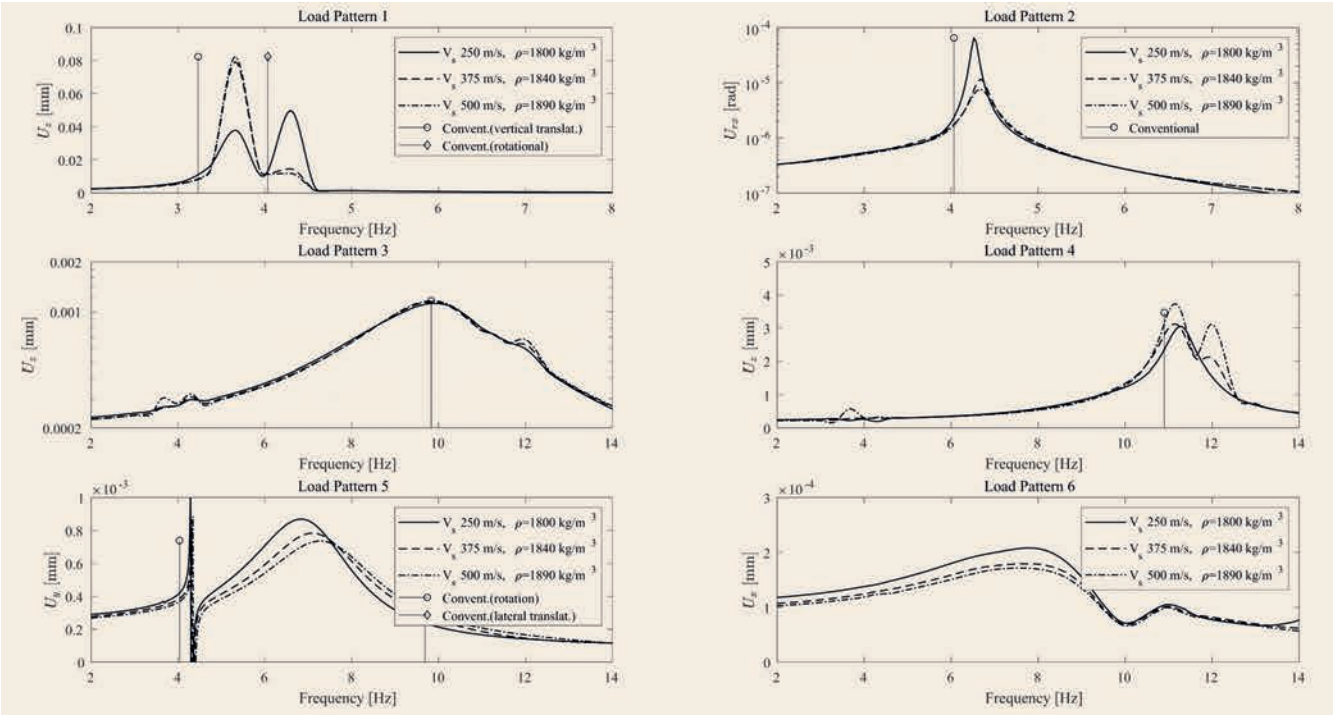

Fig. 10. Comparison of displacement response magnitude for six load patterns of bridge model 2 (L = 35 m, curved R = 400 m) with different backfill soil properties *Source: H. D. B. Aji, M. B. Basnet, F. Wuttke*

gitudinal translational mode shape is obtained from conventional approach due to the fixed restrains used in the model.

For bridge model with curved alignment, load pattern 1 generates 2 mode shapes with closely spaced resonant frequencies. These mode shapes are the 1st and 2nd mode shapes in Figures 4(a) and 4(b), respectively. Comparing Figures 5 and 7, it can be seen that the range of alteration of the resonant frequencies is lower on longer span bridge. For load pattern 1, 2, and 5, where the same movement mode is shared between both abutments, softer underlying soil provides less restraining effect and thus, lower resonant frequency and higher damping are observed. This restraining effect patterns are less clear in shorter bridge for load

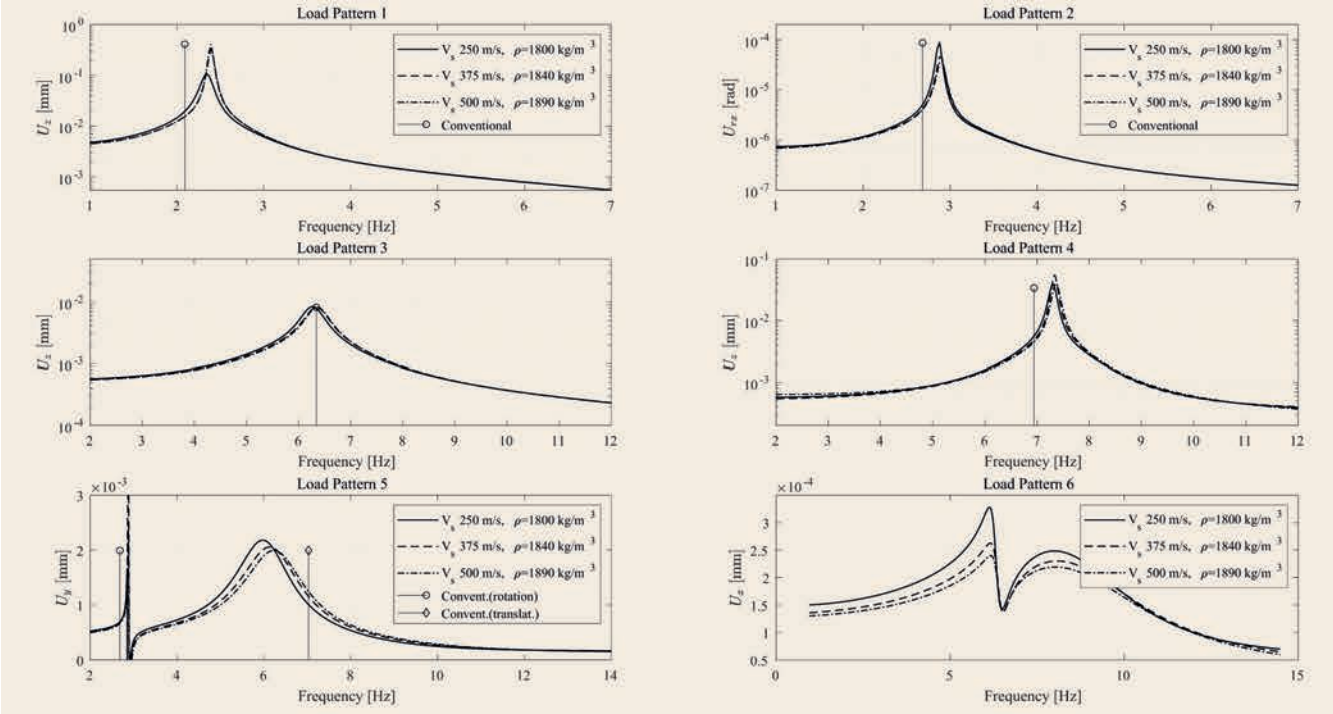

Fig. 11. Comparison of displacement response magnitude for six load patterns of bridge model 3 (L = 45 m, straight) with different backfill soil properties *Source: H. D. B. Aji, M. B. Basnet, F. Wuttke*

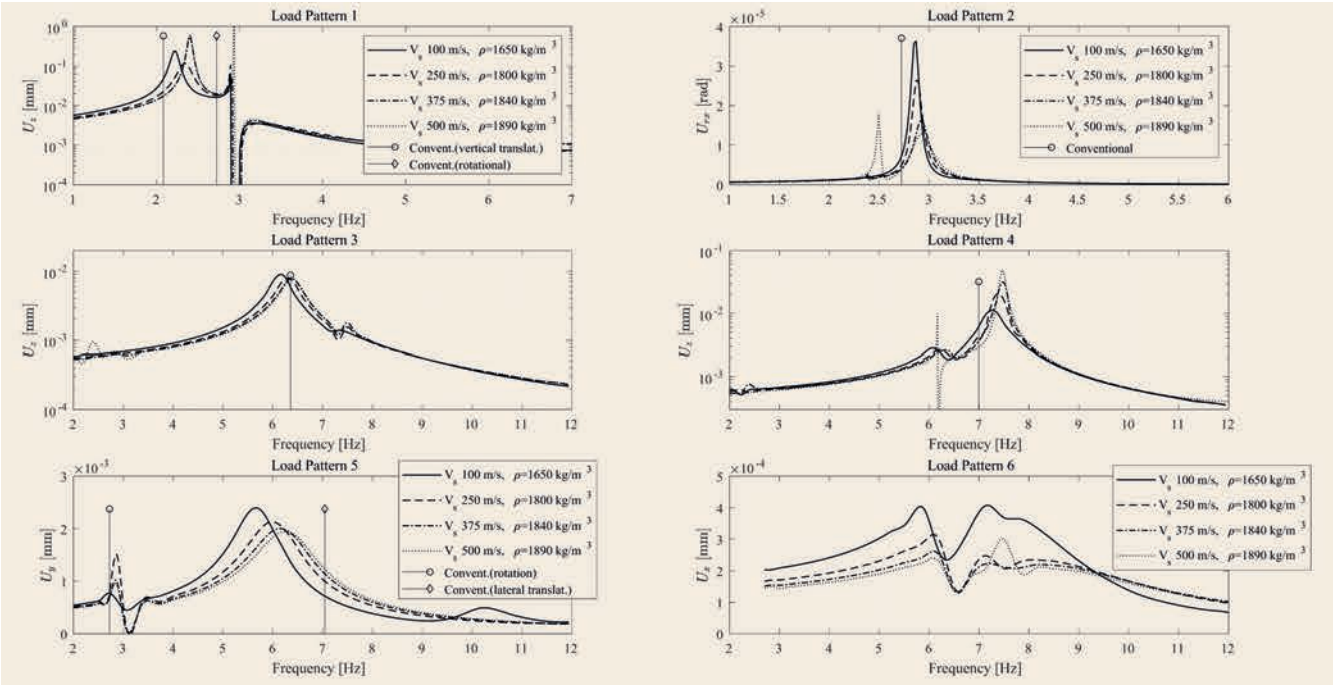

Fig. 12. Comparison of displacement response magnitude for six load patterns of bridge model 4 (L = 45 m, curved R = 400 m) with different backfill soil properties *Source: H. D. B. Aji, M. B. Basnet, F. Wuttke*

pattern 3 and 4, where different movement modes are experienced by each abutment, although the damping pattern is still clear. Exception is found on the longitudinal mode shape generated by load pattern 6 where the higher horizontal restrain from stiffer soil yields higher damping but also higher frequency. The responses of the coupled system due to the load patterns 1 to 4 are dominated by the stiffness of the superstructure while the responses due to load patterns 5 and 6 are controlled by the soil-structure interaction and thus, higher resonant frequencies alteration are observed from these load patterns.

In Figures 9 and 10, the damping effect coming from softer backfill is clear in load patterns 1, 2, and 4; opposite effect is found in load pattern 5 and 6; and no significant effect found from the response to load pattern 3. In all considered mode sha-

pes, the alteration of the resonant frequencies due to the backfill are less pronounced than the effect observed to the underlying soil. This is due to the role of the wingwalls which stiffness is much higher than the considered backfill and thus, they dominate the force transfer from the superstructure to the underlying soil. In the mode shapes 5 and 6, where higher soil-structure interaction is incorporated, the stiffer backfill provides higher damping.

6 Conclusions

A numerical study utilizing 3-dimensional hybrid BEM-FEM formulation to solve dynamic soil-structure interaction of four typical integral bridges is presented. Focus is given on the influence of the underlying soil and backfill to the response of the bridge-soil system to external time-harmonic load patterns, which are used to generate the mode shapes of the coupled system. Withal, the effect of the span and curvature is briefly explored.

The results show that the underlying soil has strong influence on the resonant frequencies and damping of the coupled system, especially on shorter bridge. The range of resonant frequency alteration is found to be significantly higher in mode shapes that incorporate more soil-structure interaction compared to the mode shapes dominated by the flexural stiffness of the superstructure. It is also found that the consideration of the abutment wingwalls in the modelling influences the results as they may act as dominating interaction links between the soil and superstructure. Under this condition, the backfill has small influence on the resonant frequencies although the effect on damping may be high. The bridge models with curved alignment are more prone to a shift of mode shape due to the geometry of the superstructure.

Literature

[1] ABAQUS Manual, A.U.S. Dassault Systemes Simulia Corp. Providence, RI, USA, 2008.

[2] *Aji, H. D. B.:* Numerical study of cyclic thermo-mechanical ratcheting effects on backfill of integral bridges. Bauhaus-Universität Weimar, Master Thesis, 2014.

[3] *Arsoy, S.; Barker, R. M.; Duncan, J. M.:* The behavior of integral abutment bridges. Report No. FHWA/VTRC 00-CR3. Virginia Transportation Research Council, USA, 1999.

[4] *Aviram A.; Mackie, K. R.; Stojadinovic, B.:* Effect of abutment modelling on the seismic response of bridge structures. *In:* Earthquake Engineering and Engineering Vibration, Vol. 7 (2008), Iss. 4, pp. 395-402.

[5] *Barbosa, A. R.; Silva, M. A. G.:* Bridge abutment interaction under seismic loading. *In:* Proceedings of the 2nd International Conf. on Structural Condition Assessment, Monitoring and Improvement, Changsha, 2007.

[6] *Basnet, M. B. et al.:* Wave propagation through poroelastic soil with underground structures via hybrid BEM-FEM. *In:* ZAMM-Zeitschrift für Angewandte Mathematik und Mechanik, Vol. 98 (2018), Iss. 8, pp. 1390-1411.

[7] *Dominguez, J.:* Boundary elements in dynamics. WIT Press, Southampton, 1993.

[8] EN 1997–1. Eurocode 7: Geotechnical design – Part 1: General rules. European Committe for Standardization (CEN), 2004.

[9] *Erhan S.; Dicleli, M.:* Effect of dynamic soil-bridge interaction modeling assumptions on the calculated seismic response of integral bridges. *In:* Soil Dynamics and Earthquake Engineering, Vol. 66 (2014), pp. 42-55.

[10] *Feldmann, M. et al.:* Economic and durable design of composite bridges with integral abutments. European Commission-Research Fund for Coal and Steel Unit (RFCS), EUR 24224, European Commission, 2010.

[11] *Gazetas, G.:* Formulas and charts for impedances of surface and embedded foundations. *In:* Journal of geotechnical engineering, Vol. 117 (1991), Iss. 9, pp. 1363-1381.

[12] *Goel, R. K.:* Earthquake characteristic of bridges with integral abutments. *In:* Journal of Structural Engineering, ASCE, Vol. 123 (1997), Iss. 11, pp. 1435-1443.

[13] *Goel, R. K.; Chopra, A. K.:* Evaluation of bridge abutment capacity and stiffness during earthquakes. *In:* Earthquake Spectra, Vol. 13 (1997), Iss. 1, pp. 1-21.

[14] *Hassiotis, S. et al.:* Evaluation of Integral Abutments. Report No. FHWA-NJ-2005–025, New Jersey Department of Transportation, Division of Research and Technology, USA; and U.S. Department of Transportation, Federal Highway Administration, 2006.

[15] *Kamali, A. Z.:* Dynamic soil-structure interaction analysis of railway bridges. Stockholm, KTH Royal Institute of Technology, Dissertation, 2018.

[16] *Karantzikis, M.; Spyrakos, C.:* Seismic analysis of bridges including soil-abutment interaction. *In:* Proceedings of the 12th World Conference on Earthquake Engineering, Auckland, 2000, Computer file No 2471.

[17] *Lan, C.:* On the Performance of Super-Long Integral Abutment Bridges – Parametric Analyses and Design Optimization. University of Trento, Engineering of Civil and Mechanical Structural Systems, Dissertation, 2012.

[18] *Martinez, A.; Mateo, J.; Alarcon, E.:* Dynamic soil-structure interaction in bridge abutments. *In:* Advances in Boundary Element Methods, 1996, pp. 135-143.

[19] *Moehle, J. P.; Eberhard, M. O.*: Earthquake damage to bridges. Bridge Engineering Handbook, CRC Press, Boca Raton, 2003.

[20] *Spyrakos, C.; Loannidis, G.:* Seismic behavior of a post-tensioned integral bridge including soil-structure interaction (SSI). *In:* Soil Dynamics and Earthquake Engineering, Vol. 23 (2003), pp. 53-63.

[21] *Vasilev, G. et al.:* Soil-structure interaction using BEM-FEM coupling through ANSYS software package. *In:* Soil Dynamics and Earthquake Engineering, Vol. 70 (2015), pp. 104-117. ABAQUS Manual, A.U.S. Dassault Systemes Simulia Corp. Providence, RI, USA, 2008.

[22] *Waldin, J.; Jennings, J.; Routledge, P.:* Critically damaged bridges and concepts for earthquake recovery. *In:* Proceedings of the New Zealand Society for Earthquake Engineering Annual Conference, 2012, pp. 1-8.

[23] *Werner, S. D.; Beck, J. L.; Levine, M. B.:* Seismic refraction evaluation of Meloland road overpass using the 1979 Imperial Valley earthquake records. *In:* Earthquake Eng. and Structural Dynamics, Vol. 15 (1987), pp. 249-274.

[24] *Werner, S. D.; Beck, J. L.; Nisar, A.:* Dynamic tests and seismic excitation of a bridge structure. *In:* Proceedings of the 4th U.S. Natl Conference on Earthquake Engineering 1, 1990, pp. 1037-1046.

[25] *Wilson, J. C.; Tan, B. S.:* Bridge abutments: assessing their influence on earthquake response of Meloland road overpass. *In:* Journal of Engineering Mechanics, ASCE, Vol. 116 (1990), Iss. 8, pp. 1838-1856.

H. D. B. Aji

hendrawan.aji@ifg.uni-kiel.de

Source: H. D. B. Aji

M. B. Basnet

min.basnet@ifg.uni-kiel.de

Prof. Dr.-Ing. Frank Wuttke

frank.wuttke@ifg.uni-kiel.de

Christian-Albrechts-Universität zu Kiel
Ludewig-Meyn-Straße 10, 24118 Kiel

Study of the Seismic Performance of Composite Shear Walls with Embedded Steel Truss For Use in High-rise Buildings

A. Khazei, A, Kolbitsch. R. Heuer

ABSTRACT The composite wall with encased steel braces (ESB wall) is a novel type of steel–concrete composite wall that consists of a steel braced frame embedded in reinforced concrete. This arrangement is supposed to enhance the seismic performance of the wall, as the steel columns encased in the boundary elements can increase the flexural strength of the wall and the steel braces encased in the web can increase the shear strength. ESB walls have seen use in super tall building structures constructed in regions of high seismicity. The ESB walls are commonly used on stories where the shear force demand is very high. Currently, no design guidelines exist for the design of ESB Walls in the Eurocode. More research is required before a distinct set of guidelines can be prescribed for the design of ESB Walls. The present research will investigate behavior of composite walls with encased steel braces (ESB walls). Time history analysis will be performed to examine the shear strength and stiffness of the ESB walls. In this study, two frames with three floors and five floors will be modeled in ABAQUS software. Then the X- shaped braces and inverted V brace is added to frames. Later, reinforced concrete shear wall will be added to braced frames, so the steel braces encased in the reinforced concrete shear wall. Time history analysis, on the braced frames will be done Compare and note with each other.

The results of the study are in good agreement with those of previous studies. However, none of these studies examined the effect of using V- and X-shaped struts and shear walls simultaneously, nor did they examine which struts reinforce the structures more strongly against earthquake vibrations. This has led the study to examine the effect of these reinforcements under various earthquakes. In future studies, reinforced concrete structures can also be used in addition to steel structures, and the results can be compared. In addition, these braces can also be used in other parts of the building. To meet this objective, one can use the very important data provided in this thesis, and ultimately better and more accurate results can be extracted using this approach.

The main aim of this thesis is to study the effect of increasing the number of floors on how to extend the stress on the building structure. To this end, the number of floors increased from three to five. Therefore, it can be concluded that an increase in the number of floors also more than 5 storey causes stress values, but these modes are quite consistent with the three- and five-storey buildings.

1 Introduction

Shear walls have long been used as resistance systems. Some of the most commonly used shear walls in multi-storey buildings are reinforced concrete shear walls (RC walls) and steel plate shear walls (SPSWs). Various types of steel and concrete composite walls have been developed and used in seismic zones. Nie et al. [1] investigated the seismic behaviour of high-strength composite walls composed of concrete filled steel tubular (CFT) columns at the two boundaries and high-strength concrete filled double-steel-plate wall bodies. Rafiei et al. [2] and Hossain et al. [3] investigated the behaviour of composite shear walls consisting of two skins of profiled steel sheeting and an infill of concrete under in-plane monotonic and cyclic loading, respectively, demonstrating more ductile behaviour and a higher energy absorbing capacity. Chen et al. [4] studied the double steel plate-high strength concrete composite walls with concrete filled steel tube boundary elements, showing high strength and excellent deformation capacity.

Recently, a new type of composite shear wall that includes encased steel braces (ESB) has been proposed for better seismic performance of structures. ESB walls have been used in super-high constructions constructed in regions of high seismicity. The ESB walls are commonly used on stories where the demand for shear force is very high (for example, the walls of the core on the lower floors or on the outrigger story). Experimental and analytical studies on composite shear walls have been limited to static and quasi-static cyclic loads. ESB walls have not been studied under real seismic loads. So far, no comprehensive research has been conducted on ESB walls seismic loading. The research objective of this study was to evaluate the seismic performance of ESB walls. A nonlinear finite element model was developed to study the behaviour of ESB walls.

2 Literature Review

Dan et al. (2011) theoretically and experimentally examined the nonlinear behaviour of composite shear walls with vertical steel concealed profiles in their work. To study the behaviour of the concrete walls reinforced by vertical steel sections, a theoretical and experimental program was developed in the Civil Engineering Department at the Politehnica University of Timisoara, Romania.

According to Tomii [6] and Gao [7], as a part of the overall frame system, the framed shear wall is expected to carry a larger portion of the horizontal load according to its high stiffness. A finite element (FE) model is developed to model the behaviour of SRC–RC walls under constant axial load and lateral loading. A series of tests, consisting of six shear wall instances, were executed under cyclic loading conditions to investigate the strength, ductility, and energy dissipation of them, as well as to verify the FE model.

The numerical modelling of sheet steel reinforced concrete shear walls was studied by Nguyen and Whittaker (2017). All

Table 1. Values of the parameters describing the recommended Type 1 spectral shape [48]

Ground type	S	T_B	T_C	T_D
A	1.0	0.15	0.4	2.0
B	1.2	0.15	0.5	2.0
C	1.15	0.2	0.6	2.0
D	1.35	0.2	0.8	2.0
E	1.4	0.15	0.5	2.0

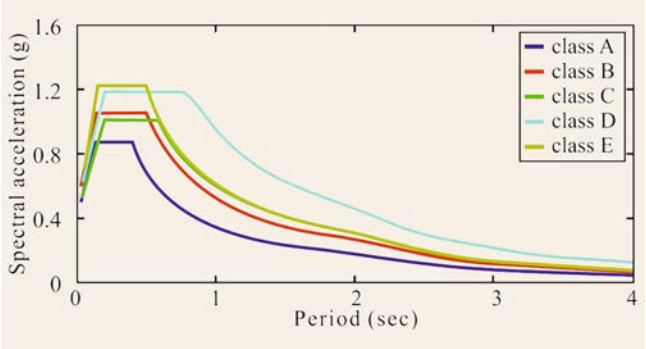

Fig. 1. Elastic response spectra for different site soil classes, based on the EC8 *Source: [48]*

four walls had an aspect ratio (height-to-length, H = L) of 1.0. Each SC wall was installed on top of a re-usable foundation block. The forecasted responses, including global force displacement relationships, damage to infill concrete and steel faceplates, shearing force contributions, and connector behaviour, are in good accord with the measured data.

3 Finite Element Modeling

Modelling of Finite Element (FE) composite walls for the development of numerical models based on experimental program was carried out. One goal of this study was to develop a reliable finite element model that can simulate the behaviour of composite shear wall. Based on the finite element model, a parametric study was performed to investigate the behaviour of the wall with variable steel strength, concrete strength, and location/orientation of intermediate steel-concrete connectors.

In this paper, two frames with three floors and five floors were modelled in ABAQUS software. Then, the X- shaped braces and inverted V brace were added to the frames. A time history analysis was performed on the braced frames. Afterwards, reinforced concrete shear walls were added to braced frames, so that the steel braces were encased in the reinforced concrete shear wall. This was supposed to enhance the seismic performance materials, as steel columns encased in flexural strength of the boundary walls and laminated steel braces on the web can increase shear strength. The frames' behaviour was evaluated before and after the addition of the concrete shear wall.

3.1 Based on Eurocode-8 Part 1 (EC-8) [48], the elastic response spectrum, Sa (T), can be defined by Eq.

$$S_a(T) = \begin{cases} a_g S[1 + (\eta 2.5 - 1)] & 0 \le T \le T_B \\ a_g S \eta 2.5 & T_B \le T \le T_B \\ a_g S \eta 2.5 \left[\frac{T_C}{T}\right] & T_C \le T \le T_D \\ a_g S \eta 2.5 \left[\frac{T_C T_D}{T^2}\right] & T_D \le T \le 4s \end{cases} \quad (1)$$

Where T stands for the vibration period of a linear SDOF system; S is the soil factor; T_B, T_C are the limiting periods of the constant spectral acceleration branch; T_D is the value defining the beginning of the constant displacement response range of the spectrum; η is the damping correction factor with a reference value of η = 1 for 5% viscous damping; a_g is the design ground acceleration on type A ground which is defined according to seismic hazard level of the site. In this study, a_g is chosen as 0.35 g.

The values of the periods T_B, T_C, and T_D and of the soil factor S describing the shape of the elastic response spectrum depend upon the ground type. In **Table 1**, the specific values that determine the spectral shapes for type 1 spectra have been listed. The resulting spectra, normalized by a_g, are plotted in **Figure. 1.**

The selection and scaling process performed were based on EC 8 Part 1. Three pairs of records were selected. Then, the horizontal components of each record were scaled with same scale factor. Selected records are summarised in **Table 2**. The scaling process that was performed based on EC 8 Part 1 is shown in **Figure 2**.

4 Modeling in ABAQUS

4.1 The FE Model

FEM is a numerical solution method. In the finite element method, the geometric model is divided into smaller components

Table 2. Selected Rekords [50]

Record	Direction	Earthquake Magnitude	Distance (km)	DT (sec)	PGA (cm/sec2)	PGV (cm/sec)	PGD (cm)
Imperial Valley, 1940, El Centro	X	6.9	10	0.02	452.03	62.40	27.73
Imperial Valley, 1940, El Centro	Y	6.9	10	0.02	662.88	59.89	14.28
Loma Prieta, 1989, Gilroy	X	7	12	0.02	652.49	79.14	28.30
Loma Prieta, 1989, Gilroy	Y	7	12	0.02	950.93	56.02	16.45
Northridge, 1994, Sylmar	X	6.7	6.4	0.02	558.43	80.19	17.33
Northridge, 1994, Sylmar	Y	6.7	6.4	0.02	801.44	118.93	26.90

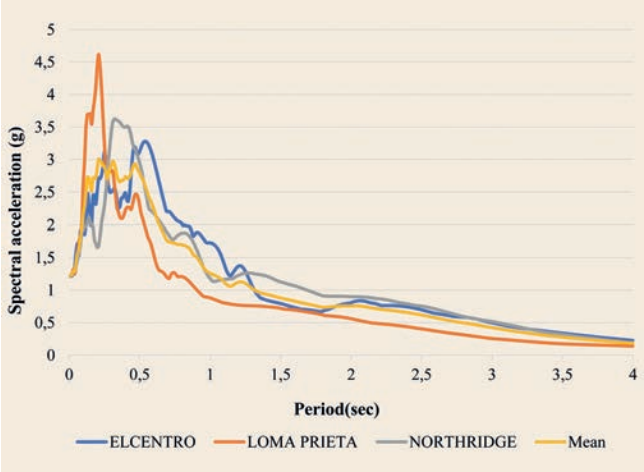

Fig. 2. Ground motion spectra *Source: [55]*

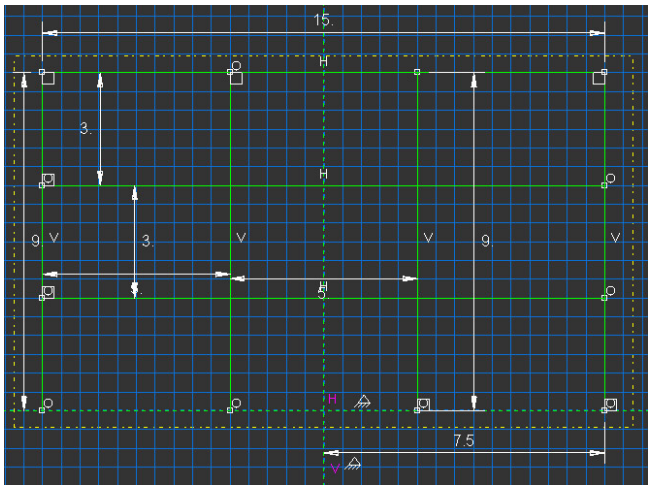

Fig. 3. Dimensions and sizes used to model three-storey building *Source: [55]*

called elements, and an analysis was performed done of the model based on the elements of division. To investigate the behaviour of composite steel shear walls, a suitable mathematical model is required. According to features that contain the finite element method to solve complex problems, in this study, the finite element method was used for verification. This research attempts to simulate the results of a laboratory experiment with program ABAQUS. This test program consisted of 2 parts. In Parts 1 and 2, seven to eight copies were tested.

4.2 Introduction

Earthquakes are one of the most destructive factors of many building structures in different parts of the world. This phenomenon causes irreparable loses to life and property each year. However, the number of these loses can be significantly reduced by changing the building structure. This has led many researchers to perform many studies on the seismic vulnerability of structures caused by destructive earthquakes. No study has investigated the impact of using three types of braces (V, X, and shear walls) together or addressed the question of which braces reinforce the structure against earthquake vibrations. This study examines the effect of these reinforcements under different earthquakes.

4.3 3D Modeling of building structures

Wire elements are used to model building structures. Two-dimensional view of a three-storey building can be seen in **Figure 3**. Each storey is three meters high. Also, in this figure, the three-dimensional view of the building is shown in as normal and with two models of brace and shear wall (**Figure 4**). The same sizes and dimensions are used to construct a five-storey building (**Figure 5**).

In ABAQUS, there are three ways to apply ground foundatio n (**Figure 6**):

1. Place a plate under the structure and Place the panel at the base of the building.
2. Connect the uprights: In this case, all the stairs of the building are connected, and the movement is applied only to the center of the floor of the building.
3. The shift can be applied equally to all bases. We actually apply the earth reaction to the foundations of the building, and the earth is eliminated.As follows **Figure 7.**

To connect the profiles with each other we use in our Models tie constraint ties two separate surfaces together so that there is no relative motion between them. This type of constraint allows you to fuse together two regions even though the meshes created

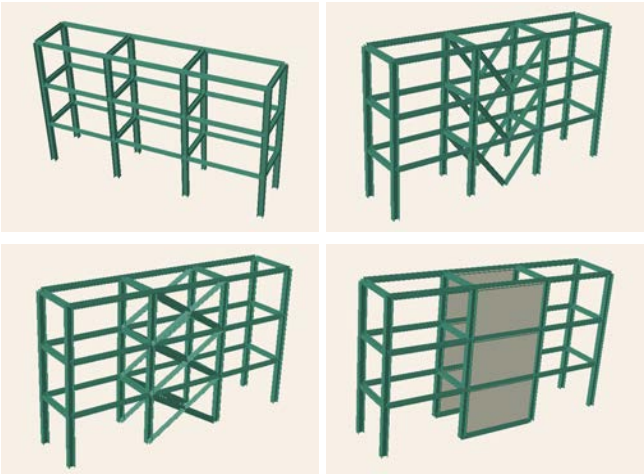

Fig. 4. three-storey building model *Source: [55]*

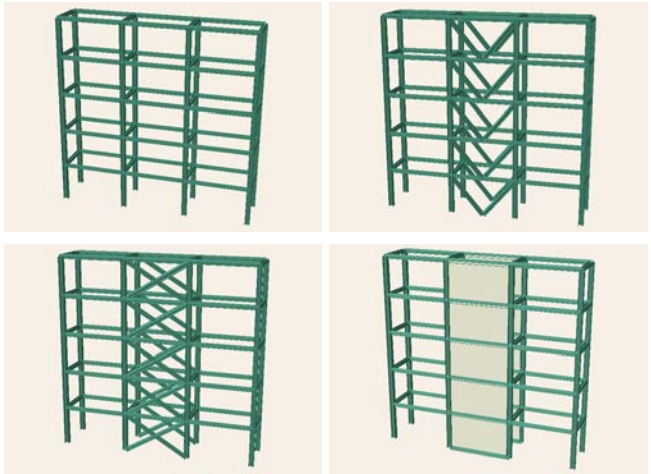

Fig. 5. five-storey building model *Source: [55]*

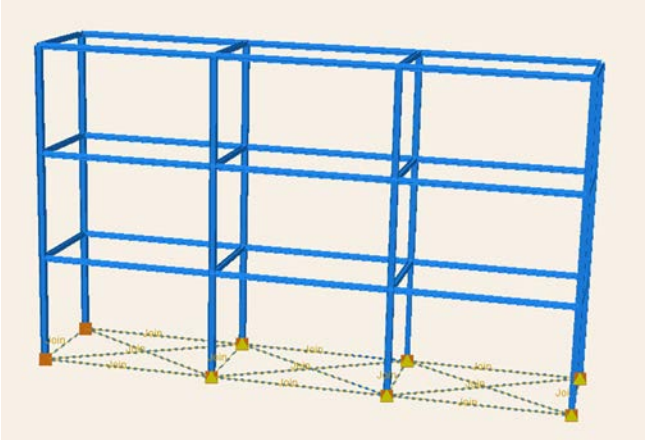

Fig. 6. Ground foundation with Connect the uprights *Source: [55]*

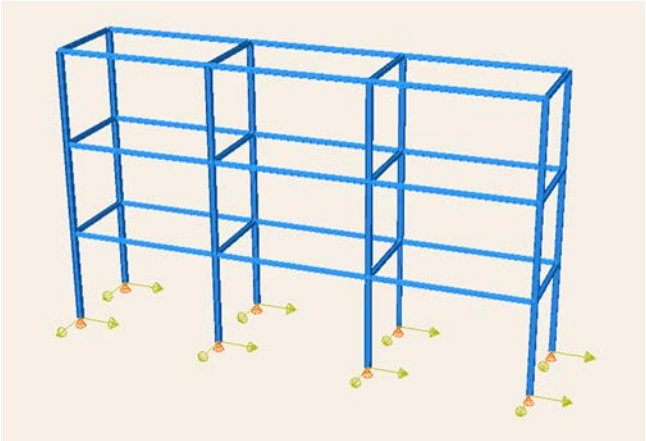

Fig. 7. Ground foundation with apply equally to all bases (Columns) *Source: [55]*

Table 3. Table of the material used specifications [55]

Steel mechanical properties with regard to true stress and Strain	
Density	80,5
Elastic modulus	210 Gpa
Poisson´s ratio	0.30

on the surfaces of the regions may be dissimilar. meaning Abaqus generally welds these parts together itself it does not allow the junction to move.

4.4 Profiles and mechanical properties used

Two types of profiles were used order to model the structure of the building. One type of profile was used for building foundations and the other type for horizontal beams and building reinforcements. IPB180 profiles were used for vertical foundations and IPB140 profiles for horizontal ones. In order to define the mechanical properties of the building structure, steel with the specifications in **Table 3** is used. Load and boundary conditions.

4.5 Load and boundary conditions

Following the complete modeling of three and five-story buildings in Abaqus software, it is now time to apply the load and boundary conditions to the building. To this end, the acceleration recorded by the earthquake accelerometer sensors in the El Centro, Loma Prieta and Northridge areas is applied to the building foundation. These accelerometers have recorded the accelerations applied in the directions x and y. In **Figure 8**, the acceleration applied in the directions x and y for the El Centro area are shown.

4.6 Finite element analysis of three-story building

When the accelerogram is used in the El Centro area. As is evident, the building is not damaged by applying this earthquake to the structure, but a lot of force and pressure are applied to the building foundations. By applying reinforcement to the structure of the building, the stress value is regularly reduced. In fact, by applying the V-shaped reinforcement to the structure, the stress is significantly reduced compared to the normal mode, and by applying X-shaped reinforcement, this stress will be less than that of the V-shaped reinforcement. Finally, by applying the shear wall to the structure, the stress value reaches its lowest extent, and much less stress is applied to the structure of the building than the two V and X-shaped reinforcement models.

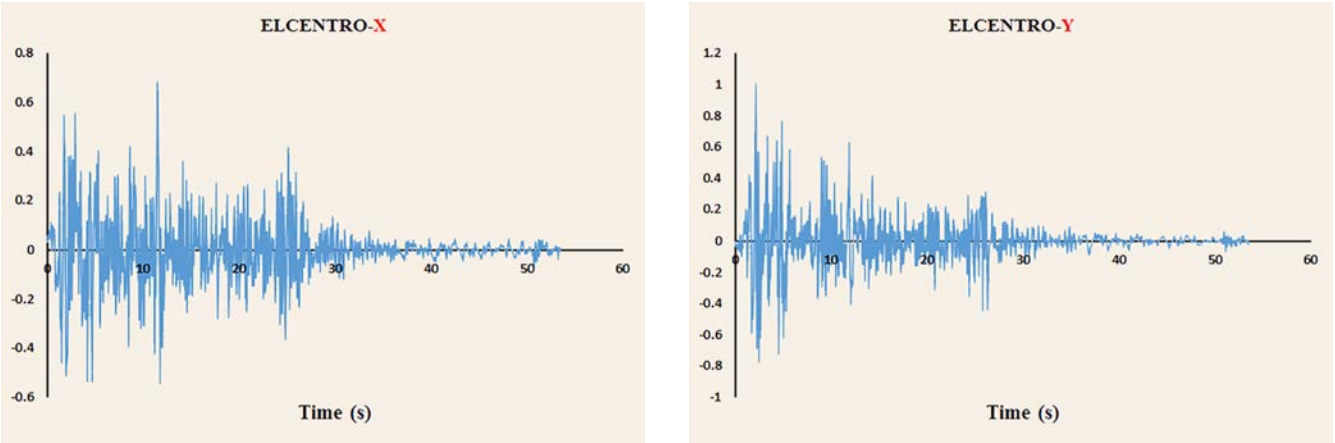

Fig. 8. the earthquake applied in directions x and y to the building foundation for the EL CENTRO area *Source: [55]*

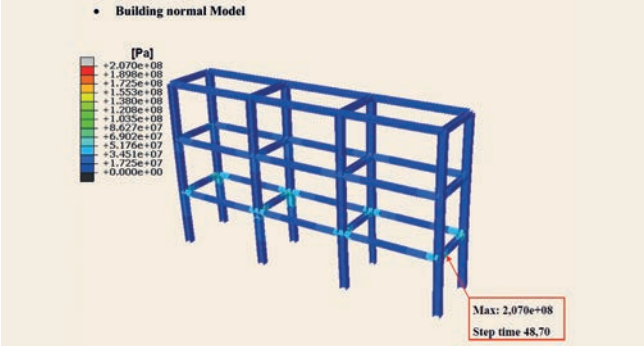

Fig. 9. Stress contour for three-storey building in normal model *Source: [55]*

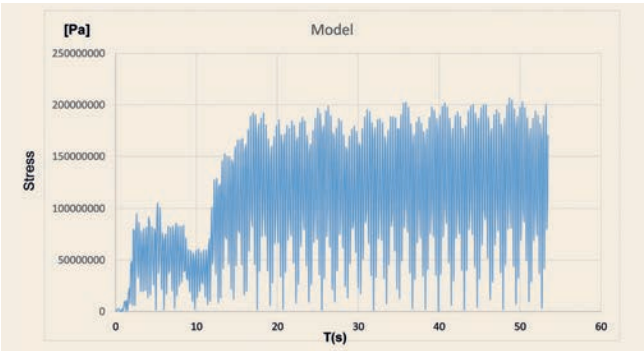

Fig. 10. The total stress time course for those nodes in which the maximum values in normal model *Source: [55]*

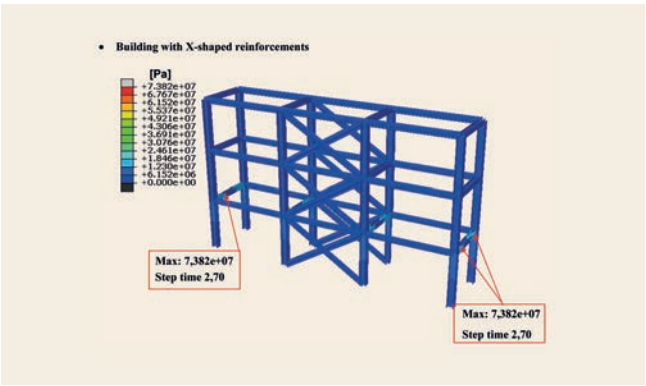

Fig. 13. Stress contour for three-storey building with X-shaped reinforcements *Source: [55]*

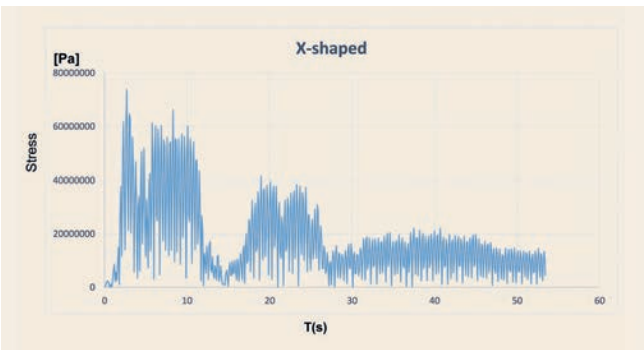

Fig. 14. The total stress time course for those nodes in which the maximum values in model with X-shaped reinforcements *Source: [55]*

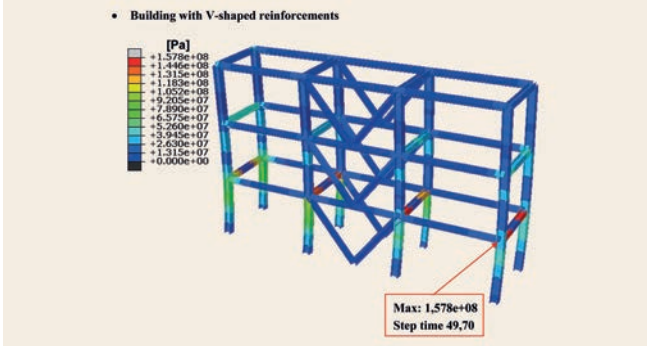

Fig. 11. Stress contour for three-storey building with V-shaped reinforcements *Source: [55]*

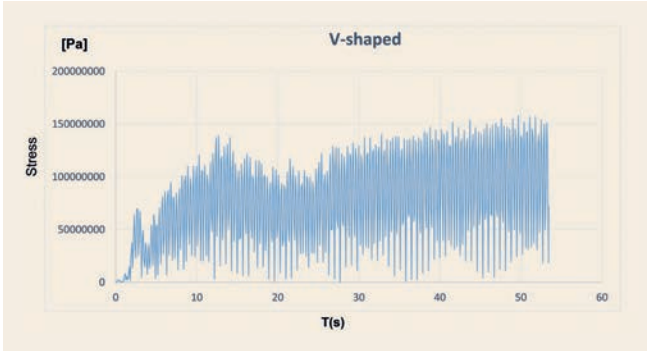

Fig. 12. The total stress time course for those nodes in which the maximum values in model with V-shaped reinforcements *Source: [55]*

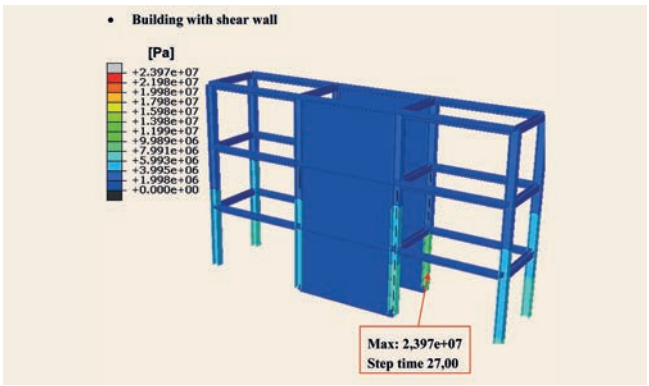

Fig. 15. Comparison of stress results for three-storey building with shear wall *Source: [55]*

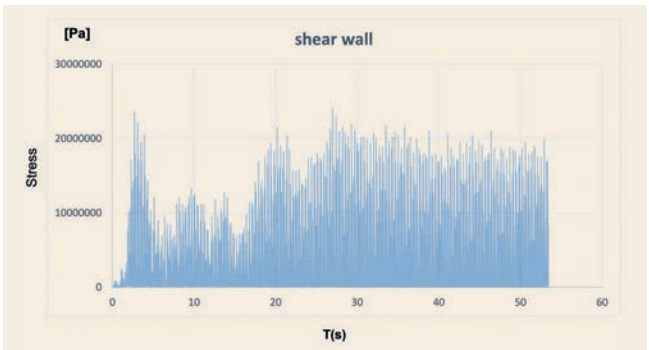

Fig. 16. The total stress time course for those nodes in which the maximum values in model with shear wall *Source: [55]*

Table 4. Table of Comparison of stress results El Centro [55]

Stress (Mpa)	Building type
207	Building normal Model
157.8	Building with V-shaped reinforcement
73.82	Building with X-shaped reinforcement
23.97	Building with shear wall

Table 5. Table of Comparison of stress results Loma Prieta area [55]

Stress (Mpa)	Building type
75.15	Building normal Model
67.15	Building with V-shaped reinforcement
32.71	Building with X-shaped reinforcement
15.98	Building with shear wall

Table 6. Table of Comparison of stress results Northridge area [55]

Stress (Mpa)	Building type
99.19	Building normal Model
60,33	Building with V-shaped reinforcement
45.54	Building with X-shaped reinforcement
22.68	Building with shear wall

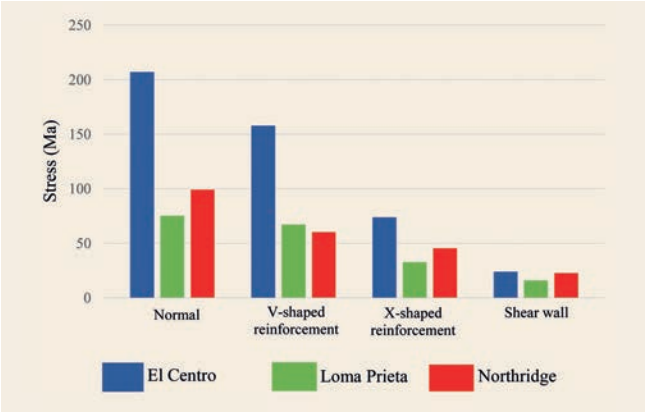

Fig. 17. comparing the results of the obtained stresses *Source: [55]*

4.6.1 El Centro area

In the **Figures 9 until 16**, the stress contours for the three-storey building are shown, when the accelerogram is used in the El Centro area. As is evident, the building is not damaged by applying this earthquake to the structure, but a lot of force and pressure are applied to the all building Columns. By applying reinforcement to the structure of the building, the stress value is regularly reduced. In fact, by applying the V-shaped reinforcement to the structure, the stress is significantly reduced compared to the normal mode, and by applying X-shaped reinforcement, this stress will be less than that of the V-shaped reinforcement. Finally, by applying the shear wall to the structure, the stress value reaches its lowest extent, and much less stress is applied to the structure of the building than the two V and X-shaped reinforcement models.

4.6.1.1 Comparison of stress results for three-storey building in the El Centro area

The maximum stresses applied to the building structure are presented in the **Table 4**. As it is obvious, the stress value decreases as a result of improvement of building reinforcements. This means that the structure needs more intense pressures and vibration so that it can enter the plastic zone and thus fracture zone. For modeling this structure, steel with a yield stress of 450 MPa has been used. If the structure is without any reinforcement, the building only needs 243 MPa to enter the plastic deformation zone, but if a shear wall is used, this difference reaches 426 MPa.

4.6.2 Loma Prieta area

In this part, the modeling and loading method is the same as in the previous part. Due to the lack of space to display all models, only here the test results are shown.

4.6.2.1 Comparison of stress results for three-storey building in the Loma Prieta area

The maximum stresses obtained for building structure in the event of vibrations applied in the Loma Prieta area are given in the **Table 5**. As it is obvious, in this case applying the reinforcement to the structure of the building will reduce the amount of stress and thus the structure remains healthy.

4.6.3 Northridge area

In this part , the modeling and loading method is the same as in the part 4.6.1. Due to the lack of space to display all models, only here the test results are shown.

4.6.3.1 Comparison of stress results for three-storey building in the Northridge area

The maximum amount of stresses applied to the building structure is given in the **Table 6**. In this area, like the other two areas, the amount of stressed to the structure decreases regularly by improving the reinforcements.

4.6.4 General comparison for three-story building

In the Figure 17, the maximum stresses applied to the building structure for the three areas (El Centro, Loma Prieta and Northridge) and for the four types of structures are depicted. As is seen in this figure, when the earthquake occurs in the El Centro area, the stress is higher than the other two. This is due to the severity of the earthquake in the area. As it is clear from this diagram, by varying the reinforcement from V to X, and then to the shear wall, the applied stress in all three areas will be regularly reduced. This suggests that the use of a shear wall in the building

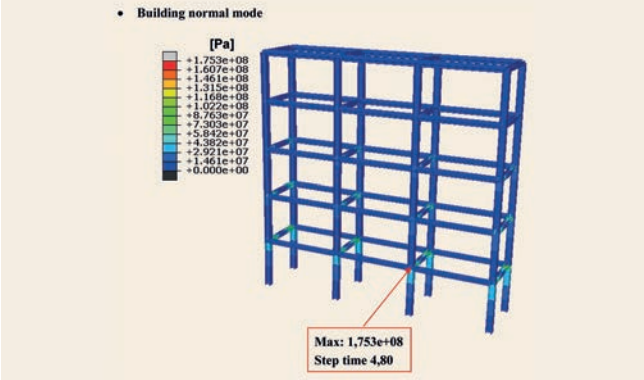

Fig. 18. Stress contour for five-storey building in normal model *Source: [55]*

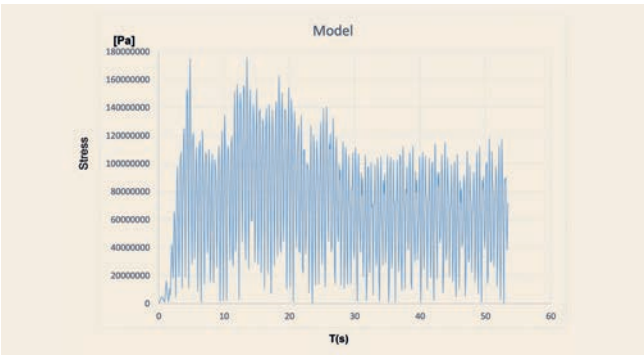

Fig. 19. The total stress time course for those nodes in which the maximum values in normal model *Source: [55]*

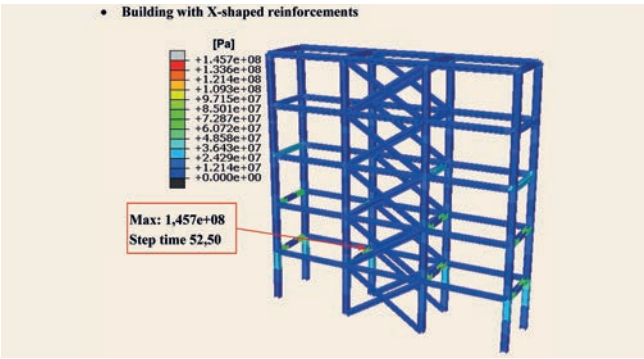

Fig. 22. Stress contour for five-storey building with X-shaped reinforcements *Source: [55]*

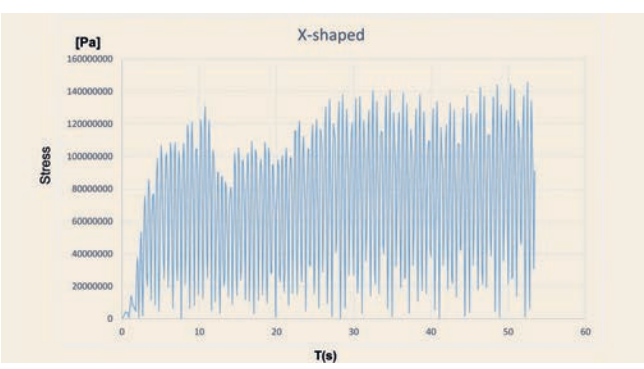

Fig. 23. The total stress time course for those nodes in which the maximum values in model with X-shaped reinforcements *Source: [55]*

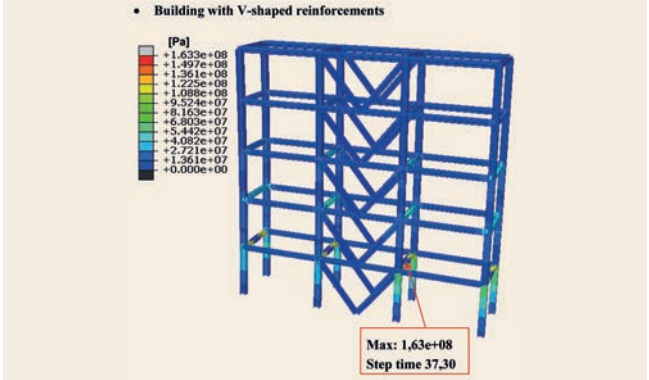

Fig. 20. Stress contour for five-storey building with V-shaped reinforcements *Source: [55]*

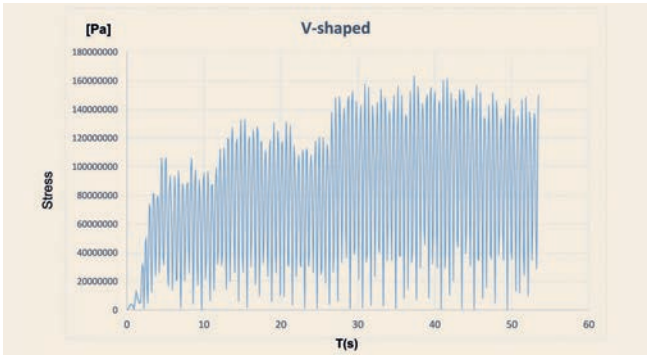

Fig. 21. The total stress time course for those nodes in which the maximum values in model with V-shaped reinforcements *Source: [55]*

Fig. 24. Stress contour for five-storey building with shear wall *Source: [55]*

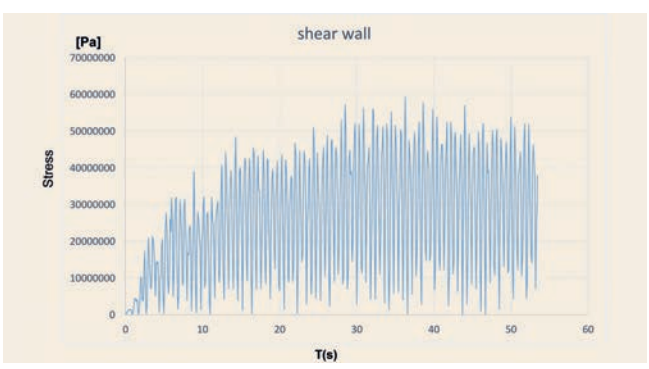

Fig. 25. The total stress time course for those nodes in which the maximum values in model with shear wall *Source: [55]*

Table 7. Table of Comparison of stress results El Centro [55]

Stress (Mpa)	Building type
175.30	Building normal Model
163.30	Building with V-shaped reinforcement
145.70	Building with X-shaped reinforcement
59.36	Building with shear wall

Table 8. Table of Comparison of stress results Loma Prieta area [55]

Stress (Mpa)	Building type
110	Building normal Model
37.85	Building with V-shaped reinforcement
24.24	Building with X-shaped reinforcement
10.29	Building with shear wall

Table 9. Table of Comparison of stress results Northridge area [55]

Stress (Mpa)	Building type
113,3	Building normal Model
100	Building with V-shaped reinforcement
96.33	Building with X-shaped reinforcement
29.01	Building with shear wall

structure has major impact on reducing the amount of stress applied to it.

4.7 Finite Element analysis of five-storey building

4.7.1 El Centro area

All the steps taken for three-storey building were also taken for five-storey building. Due to the lack of space to display all models, only the test results are shown here.

4.7.1.1 Comparison of stress results for five-storey building in the El Centro area

The maximum stresses applied to the structure of the five-story building are given in the **Table** 7. As is clear, the amount of stress decreases regularly by changing the reinforcement of the building from the V to the shear wall.

4.7.2 Loma Prieta area

In this part , the modeling and loading method is the same as in the previous part. Due to the lack of space to display all models, only here the test results are shown.

4.7.2.1 Comparison of stress results for five-storey building in the Loma Prieta area

The maximum amount of stress applied to the structure of the five-story building in the Loma Prieta area is given in the **Table 8**. As it is obvious, the amount of stress decreases regularly by changing the reinforcement from the V to the shear wall.

4.7.3 Northridge area

In this part , the modeling and loading method is the same as in the part 4.7.1. Due to the lack of space to display all models, only the test results are shown here.

4.7.3.1 Comparison of stress results for five-storey building in the Northridge area

In **Table 9**, the maximum amount of stresses applied to the structure of the five-storey building are provided. The amount of stress reaches its lowest value, when the shear wall is used in the building structure. However, the use of X-shaped reinforcements will result in a further reduction in the stress value than to the V-shaped reinforcements.

4.7.4 General comparison for five story building

The maximum stresses applied to the building structure for the three areas (El Centro, Loma Prieta and Northridge) and for four types of structures are given in **Figure 26**. In all areas, the use of a shear wall reduces the amount of stress applied to the structure significantly. This is while X-shaped reinforcements reduce the stress to a greater extent than V-shaped reinforcements.

5 Conclusion

In this research, the structure of 3– and 5-story buildings that are under the influence of various earthquakes were examined using sequential accelerograms in the areas El Centro, Loma Prieta, and Northridge. Then, two types of V- and X-shaped braces and shear walls were used to retrofit the building and prevent the development of plastic hinges in the columns at the base. To this end, the dynamic analysis in ABAQUS software was used. The results of this study indicate that the use of braces and shear walls in the building reduces the amount of stress and increases its strength to earthquakes. In fact, the shear walls reduce the tension more than X-shaped braces, and the X-shaped braces also reduce the tension more than V-shaped braces in the building structure.

3– and 5-story buildings and three types of earthquakes were used to confirm that the use of braces and shear walls reduces the amount of stress in the building structure. In all modes, the use of braces, and in particular the shear walls, resulted in a significant reduction in stress levels and more structural strength to earthquake-induced forces. Also, the X-shaped brace reduced the amount of stress more than the V-shaped brace.

Due to the fact that use of experimental techniques on 3– and 5-story buildings is very costly and time consuming, this factor prevents researchers from carrying out a comprehensive study. In this case, it is essential to use virtual simulations and computational methods, such as a finite element analysis, to examine the changes in the performance of these structures. With the advancement of analytic modelling and the finite element method as well as with the feasibility of very varied modelling of mechanical properties, analytic and numerical models become more volumi-

nous and advanced each day, are confronted with experimental techniques, and may pave the way for new research.

In this research, the structure of 3– and 5-story buildings that are under the influence of various earthquakes were examined using sequential accelerograms in the areas l Centro, Loma Prieta, and Northridge. Then, two types of V- and X-shaped braces and shear walls were used to retrofit the building and prevent the development of plastic hinges in the columns at the base. To this end, the dynamic analysis in ABAQUS software was used. The results of this study indicate that the use of braces and shear walls in the building reduces the amount of stress and increases its strength to earthquakes. In fact, the shear walls reduce the tension more than X-shaped braces, and the X-shaped braces also reduce the tension more than V-shaped braces in the building structure.

3– and 5-story buildings and three types of earthquakes were used to confirm that the use of braces and shear walls reduces the amount of stress in the building structure. In all modes, the use of braces, and in particular the shear walls, resulted in a significant reduction in stress levels and more structural strength to earthquake-induced forces. Also, the X-shaped brace reduced the amount of stress more than the V-shaped brace.

Due to the fact that use of experimental techniques on 3– and 5-story buildings is very costly and time consuming, this factor prevents researchers from carrying out a comprehensive study. In this case, it is essential to use virtual simulations and computational methods, such as a finite element analysis, to examine the changes in the performance of these structures. With the advancement of analytic modelling and the finite element method as well as with the feasibility of very varied modelling of mechanical properties, analytic and numerical models become more voluminous and advanced each day, are confronted with experimental techniques, and may pave the way for new research.

FINAL REMARK

This article is the result of my doctoral thesis, which was written in 2020 at the TU Wien, Civil Engineering and Institute for Structural Engineering, Structural Dynamics and Building Technology.
The author of the thesis is Dipl.-Ing. Dr.Techn, Ali Khazei while Prof. Anderas Kolbitsch was the supervisor and Prof. Rudolf Heuer was the reviewer.

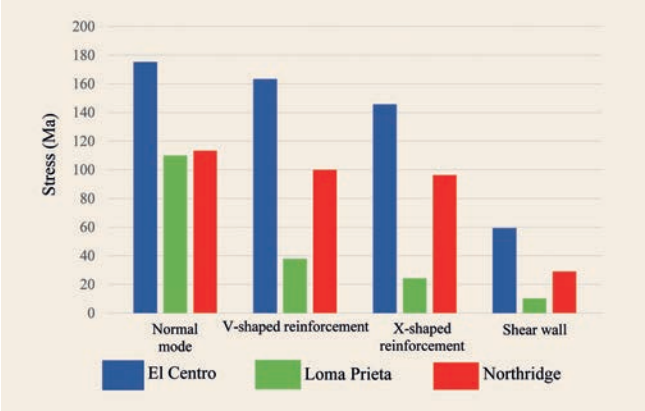

Fig. 26. Comparison of stress results for five-story building *Source: [55]*

Literature

[1] *Adams, R. D.; Cawley, P.; Pye, C. J. et al.:* A vibration technique for non-destructively assessing the integrity of structures. *In:* Journal of Mechanical Engineering Science, Vol. 20 (1978), Iss. 2.
[2] *Andersen, J. E.; Fustinoni, M.:* Structural Health Monitoring Systems. COWI-Futurtec, Lyngby, Denmark, 2006.
[3] *Brownjohn, J. M. W.; Carden, E. P.; Goddard, R. C. et al.:* Real-time performance monitoring of tuned mass damper system for a 183 m reinforced concrete chimney. *In:* Wind Engineering and Industrial Aerodynamics, Vol. 98 (2010), pp. 169-179.
[4] *Brownjohn, J. M. W., Carden, P.:* Real-time operation modal analysis of Tamar Bridge. *In:* IMAC XXVI, 2008.
[5] CIGB ICOLD: Dam monitoring General considerations. International Commission on Large Dams (1988), Bulletin 60, Paris.
[6] *Kramer, H.:* Angewandte Baudynamik, Grundlagen und Praxisbeispiele. Edition 2, Wilhelm Ernst & Sohn, Berlin, 2013.
[7] Ausführungspläne vo 1962, gezeichnet von Ooms Ittner & Cio, Köln.
[8] *Schröder, M.; Pocha, A.:* Deutscher Abbruchverband e. V., Abbrucharbeiten, Grundlagen, Planung, Durchführung. Edition 3, Verlaggesellschaft Rudolf Müller GmbH & Co. KG., Köln, 2015.
[9] *Korth, D.; Lippok, J.:* Abbrucharbeiten, Vorbereitung und Durchführung. Edition 2, VEB Verlag für Bauwesen, Berlin, 1987.
[10] *Kuttner, T.:* Praxiswissen Schwingungsmesstechnik. Fakultät für Maschinenbau, Universität der Bundeswehr München, Springer Vieweg, Neubiberg, 2015.
[11] *Hübner, E.:* Technische Schwingungslehre in ihren Grundzügen. Springer Verlag, Berlin/Göttingen/Heidelberg, 1957.
[12] National Instruments, NI DIAdem, Erste Schritte mit DIAdem, National Instruments Corporation, München, 2014.
[13] National Instruments, NI DIAdem, Daten finden, analysieren und dokumentieren, National Instruments Corporation, München, 2014.
[14] National Instruments, NI DIAdem, Daten erfassen und visualisieren, National Instruments Corporation, München, 2014.
[15] DIN 4150–3 rules, Vibrations in buildings – Part 3: Effects on structures, 2016.
[16] *Telch, F:* Vibration measurements and their assessment concerning the effect on a masonry chimney. Masterthesis, Department of Structural, Geotechnical and Building Engineering (DISEG), Politecnico di Torino, and Materials Testing and Research Institute (MPA), Karlsruher Institute of Technology, Tutors: Lacidogna G. (DISEG) and Rösch O. (MPA).
[17] *Rösch, O.:* Prüfbericht: Schwingungsmessung und Erschütterungsüberwachung an einem bestehenden Ziegelschornstein im Zuge der Rückbaumaßnahmen am Steinzeugpark in Bretten. Karlsruhe, 2017.
[18] *Das, A.:* Signal Conditioning. An Introduction to Continuous Wave, Communication and Signal Processing. Springer Verlag, Berlin – Heidelberg, 2012.
[19] *Haupt, W.:* Bodendynamik, Grundlagen und Anwendung. Friedr. Vieweg & Sohn, Braunschweig/Wiesbaden, 1986.
[20] *Korenev, B. G.; Rabinovic, I. M.:* Baudynamik. Handbuch, VEB Verlag für Bauwesen, Berlin.
[21] *Stempniewski, L.; Haag, B.:* Baudynamik-Praxis. Mit zahlreichen Anwendungsbeispielen. Bauwerk Verlag GmbH, Berlin, 2010.
[22] UNI 9916 rules, Criteri di misura e valutazione degli effetti delle vibrazioni sugli edifici, 2004.
[23] DIN EN 1996–1–1/NA, National Annex – Nationally determined parameters – Eurocode 6: Design of masonry structures – Part 1–1: General rules for reinforced and unreinforced masonry structures, 2012.
[24] DIN EN 1996–3/NA, National Annex – Nationally determined parameters –Eurocode 6: Design of masonry structures – Part 3: Simplified calculation methods for unreinforced masonry structures, 2012.
[25] DIN EN 1998–1, Eurocode 8: Design of structures for earthquake resistance – Part 1: General rules, seismic actions and rules for buildings; German version EN 1998–1:2004 + AC:2009.
[26] *Seo, J.; Varma, A. H.; Sener, K. et al.:* Steel-plate composite (SC) walls: In-plane shear behavior, database, and design. *In:* Journal of Constructional Steel Research, Vol. 119 (2016), pp. 202-215.
[27] *Wu, Y.; Kang, D.; Yang, Y.-B.:* Seismic performance of steel and concrete composite shear walls with embedded steel truss for use in high-rise buildings. *In:* Engineering Structures, Vol. 125 (2016), pp. 39-53.
[28] (GB50011–2010) Code for seismic design of buildings [in Chinese].

[29] *Nie, J.-G.; Ma, X.-W.; Tao, M.-X. et al.:* Effective stiffness of composite shear wall with double plates and filled concrete. *In:* Journal of Constructional Steel Research, Vol. 99 (2014), pp. 140-148.
[30] *Nguyen, N. H.; Whittaker, A. S.:* Numerical modelling of steel-plate concrete composite shear walls. *In:* Engineering Structures, Vol. 150 (2017), pp. 1-11.
[31] *Furlong, R. W.:* Effective Stiffness of Composite Shear Walls. *In:* Proceedings of an Engineering Foundation Conference on Composite Construction in Steel and Concrete III, Irsee, Germany, 1996.
[32] *Eom, T.-S.; Park, H.-G.; Lee, C.-H. et al.:* Behaviour of Double Skin Composite Wall Subjected to In-Plane Cyclic Loading. *In:* Journal of Structural Engineering, ASCE, Vol. 135 (2009), Iss. 10, pp. 1239-1249.
[33] *Liang, Q. Q.; Uy, B.; Wright, H. D. et al.:* Buckling of Steel Plates in Double Skin Composite Panels under Biaxial Compression and Shear. *In:* Journal of Structural Engineering, Vol. 130 (2004), Iss. 3, pp. 443-451.
[34] *Rahai, A.; Hatami, F:* Evaluation of composite shear wall behavior under cyclic loadings. *In:* Journal of Constructional Steel Research, Vol. 65 (2009), pp. 1528-1537.
[35] *Alinia, M. M.; Dastfan, M.:* Cyclic behaviour, deformability and rigidity of stiffened steel shear panels. *In:* Journal of Constructional Steel Research, Vol. 63 (2007), Iss. 4, pp. 554-563.
[36] Zhao, Q.; Astaneh-Asl, A.: Cyclic Behaviour of Traditional and Innovative Composite Shear Walls. *In:* Journal of Structural Engineering, Vol. 130 (2004), Iss. 2, pp. 271-284.
[37] *Nie, J. G.; Hu, H. S.; Fan, J. S. et al.:* Experimental study on seismic behavior of high-strength concrete filled double-steel-plate composite walls. In: Journal of Constructional Steel Research, Vol. 88 (2013), Iss. 9, pp. 206-219.
[38] *Rafiei, S.; Hossain, K. M. A.; Lachemi, M. et al.:* Composite wall with high performance concrete subjected to monotonic shear. *In:* Journal of Constructional Steel Research, Vol.107 (2015), Iss. 4.
[39] *Hossain, K. M. A.; Rafiei, S.; Lachemi, M. et al.:* Structural performance of profiled composite wall under in-plane cyclic loading. *In:* Engineering Structures, Vol. 110 (2016), Iss. 3, pp. 88-104.
[40] *Chen, L.; Mahmoud, H.; Tong, S. M. et al.:* Seismic behavior of double steel plate- HSC composite walls. *In:* Engineering Structures, Vol. 102 (2015), Iss. 11, pp. 1-12.
[41] Design of Steel Structures for Buildings is Seismic Areas 2007; ECCS Eurocode design manuals.
[42] Dassault Systèmes Simulia Corp.: ABAQUS/CAE Documentation, Version 6.8–3, Providence, RI, USA, 2008 (www.simulia.com).
[43] *Lubliner, J.; Oliver, J.; Oller, S. et al.:* A Plastic-Damage Model for Concrete. *In:* International Journal of Solids and Structures, Vol. 25 (1989), Iss. 3, pp. 299-326.
[44] *Lee, J.; Fenves, G. L.:* Plastic-Damage Model for Cyclic Loading of Concrete Structures. *In:* Journal of Engineering Mechanics, Vol. 124 (1998), Iss. 8, pp. 892-900.
[45] *Popovics, S.:* A numerical approach to the complete stress strain curve for concrete. *In:* Cement and concrete research, Vol. 3 (1973), Iss. 5, pp. 583-599.
[46] *Wang, T.; Hus, T. T. C.:* Nonlinear finite element analysis of concrete structures using new constitutive models. *In:* Computers and Structures, Vol. 79 (2001), Iss. 32, pp. 2781-2791.
[47] *Shima, H.; Chou, L.; Okamura, H.*: Micro And Macro Models for Bond Behaviour in Reinforced Concrete. *In:* Journal of the Faculty of Engineering, University of Tokyo, Vol. 39 (1987), Iss. 564, pp. 297-316.
[48] Eurocode-8: Design provisions for earthquake resistance of structures, Part1.1: General rules, seismic actions and rules for buildings, European Committee for Standardization, 2003.
[49] *Iervolino, I.; Maddaloni, G.; Cosenza, E.:* Eurocode 8 compliant real record sets for seismic analysis of structures. *In:* Journal of Earthquake Engineering, Vol. 12 (2008), Iss.1, pp. 54-90.
[50] Eurocode-8: Design provisions for earthquake resistance of structures, Part 2: bridges, European Committee for Standardization, 1998.
[51] *Arabzadeh, A.; Soltani, M.; Ayazi, A.:* Experimental investigation of composite shear walls under shear loadings. *In:* Journal of Thin - Walled Structures, Vol. 49 (2011), Iss. 8, pp. 42-54.
[52] Wikipedia:1940_El_Centro_earthquake
[53] Wikipedia: 1994_Northridge_earthquake
[54] Wikipedia: 1989_Loma-Prieta_earthquake
[55] *Flesch, R.; Pacht, H.:* Baudynamik praxisgerecht, Bd.1, Berechnungsgrundlagen.

Dipl.-Ing. Dr.Techn, Ali Khazei

Ali.khazei@yahoo.com
Tecton Consult, Engineering ZT GmbH
Nikolsdorfer 39, 1050 Wien, Österreich

Abb.: A. Khazei

Univ.Prof. Dipl.-Ing. Dr.techn. Anderas Kolbisch

andreas.kolbitsch@tuwien.ac.at
Technische Universität Wien
Institut für Hochbau und Technologie
Forschungsbereich Hochbaukonstruktion
und Gebäudetechnik
Karlsplatz 13/208–01, 1040 Wien, Österreich

Univ.Prof. Dipl.-Ing. Dr.techn. Rudolf Heuer

rudolf.heuer@tuwien.ac.at
Technische Universität Wien
Forschungsbereich Struktur Dynamik und
Risikobewertung von Tragwerken am Institut für
Hochbau, Baudynamik und Gebäudetechnik
Karlsplatz 13/208–011040, Wien, Österreich

17. D-A-CH-Tagung

Die Schweizer Gesellschaft für Erdbebeningenieurwesen und Baudynamik (SGEB) und die ETH Zürich laden zur 17. D-A-CH-Tagung ein. Diese alle zwei Jahre im Wechsel von OGE, DGEB und SGEB organisierte Veranstaltung bietet eine Plattform zum Austausch zwischen praktisch und wissenschaftlich tätigen Fachleuten, die sich mit Themen rund um Baudynamik und Erdbebeningenieurwesen beschäftigen. Die Tagung findet vom 16. bis 17. September 2021 an der ETH Zürich statt.
Kurzfassungen für Beiträge können bis 31. Dezember 2020 eingereicht werden. Besonders ermutigen möchten die Gesellschaften Einreichungen zu den folgenden Themenkomplexen:
Baudynamik: Schwingungsreduktion, Erschütterungsarmut, Personen-, Maschinen-, Verkehrs- und baustelleninduzierte Schwingungen, Anprall und Explosionen, Structural Health Monitoring; Systemidentifikation und Schadenserkennung, aktuelle Entwicklungen und Fallstudien.
Erdbebeningenieurwesen: Erdbebensicherheit von Industrie und störfallrelevanten Anlagen, Stauanlagen, Lifelines, Erdbebensicherheit sekundärer Bauteile, Risikoanalysen und Vulnerabilitätsstudien, Denkmalschutz und Erdbebensicherheit, Ingenieurseismologie, aktuelle Entwicklungen und Fallstudien zu Erdbebensicherheit von Bestands- und Neubauten.
Weitere Informationen zur Beitragseinreichung, zu den Terminen und Abläufen sind ab Oktober 2020 auf der Homepage der SGEB zu finden.
https://sgeb.ch